THE ASTROPHYSICAL JOURNAL, 414:98–111, 1993 September 1

KILOPARSEC-SCALE MOLECULAR GAS EXCITATION IN SPIRAL GALAXIES[1]

W. F. WALL,[2] D. T. JAFFE,[3] F. N. BASH,[3] F. P. ISRAEL,[4] P. R. MALONEY,[5] AND F. BAAS[6]

Received 1992 October 22; accepted 1993 March 5

ABSTRACT

We combine beam-matched ^{13}CO, ^{12}CO $J = 3 \rightarrow 2$ and $J = 2 \rightarrow 1$ line data to infer the molecular gas excitation conditions in the central 500 to 1600 pc diameters of a small sample of infrared-bright external galaxies: NGC 253, IC 342, M83, Maffei 2, and NGC 6946. We find that the central 170 to 530 pc diameter regions have typical molecular gas densities ranging from $\lesssim 10^4$ cm^{-3} (in M83) to $\gtrsim 10^5$ cm^{-3} (in NGC 253) and that, outside of these regions, the densities are likely to be $\lesssim 10^4$ cm^{-3}. The molecular clouds outside the inner 170–530 pc are at least as warm as the molecular clouds in our Galaxy. Column densities derived from integrated ^{13}CO line strengths and Hα surface brightnesses suggest that the star formation rate is enhanced in the central 170–530 pc diameters by an order of magnitude over that inferred for the outer star-forming disks in spiral galaxies. The total luminosity of each sample galaxy over all CO rotational lines is $\sim 10^5$–10^6 $L_\odot$, which is within an order of magnitude of that of the important cooling line of [C II] at 158 μm. Additional observations of the $J = 1 \rightarrow 0$ lines of $C^{18}O$ and ^{13}CO suggest that emission from the central kiloparsec of spiral galaxies may be optically thick in the ^{13}CO $J = 1 \rightarrow 0$ line. If so, estimates of molecular gas mass using ^{13}CO integrated line strengths could be too low.

The sum of the molecular line observations imply the existence of two molecular gas components: a low-density [$n(H_2) \lesssim 10^3$–10^4 cm^{-3}] component and a warm ($T_K \gtrsim 50$ K), high-density [$n(H_2) \gtrsim 10^4$–10^5 cm^{-3}] component. The warm, dense component is probably associated with star formation.

Subject headings: galaxies: ISM — galaxies: spiral — ISM: molecules

1. INTRODUCTION

Understanding large-scale star formation in galaxies requires knowledge of both the global physical conditions and global distribution of the molecular gas. The density and temperature of the gas can be strongly affected by the presence of hot young stars which can, in turn, affect the rate of future star formation. Observations of properly chosen molecular transitions can directly probe the density and temperature of the molecular gas, in addition to its spatial distribution.

Excitation of molecular gas on 100 or 1000 pc size scales is only poorly known. Most large-scale observations of galaxies are of the lowest rotational line of CO. Since this line is easily thermalized and usually optically thick, it provides little information about the excitation of the molecular gas. However, since CO is generally present wherever hydrogen is primarily H_2, this line is a good tracer of molecular material and can tell us, in a rough sense, about the distribution and amount of molecular material (Young 1987; Young & Scoville 1982a; Maloney & Black 1988). Observations of higher rotational lines (e.g., $J = 2 \rightarrow 1$ and $J = 3 \rightarrow 2$) of CO have the advantage that they can be used to set limits on density and temperature for a greater proportion of the molecular gas than that probed by lines of other molecules. Other molecules, like HCO^+ and HCN, have millimeter lines with critical densities greater than 10^5 cm^{-3}; the lines of such molecules are sensitive only to the densest portions of the molecular gas, whereas CO lines can be sensitive both to dense gas and to gas with densities lower than 10^3 cm^{-3} (depending on radiative trapping effects). A few external galaxies (e.g., M82, NGC 253, M83, NGC 6946, NGC 1068) have been observed in higher rotational lines of ^{12}CO (i.e., $J = 2 \rightarrow 1$, $J = 3 \rightarrow 2$; e.g., Knapp et al. 1980; Sutton et al. 1983; Turner, Ho, & Martin 1987b; Eckart et al. 1990; Wiklind et al. 1990; Rosenthal et al. 1988; Casoli et al. 1990; Planesas, Gómez-Gonzales, & Martin-Pintado 1989; and $J = 4 \rightarrow 3$, $J = 6 \rightarrow 5$; Güsten et al. 1993; Harris et al. 1991). However, most of these studies did not obtain observations with matched beam sizes, which are essential for intensity comparisons of the different CO lines, and did not include ^{13}CO observations. Lines of the rarer isotopic species like ^{13}CO, $C^{18}O$, and $C^{17}O$ are more directly sensitive to molecular gas density and temperature than ^{12}CO lines. Therefore, observations of two or more ^{13}CO lines (e.g., Eckart et al. 1990; Wall & Jaffe 1990; Wall et al. 1991; Tilanus et al. 1991), preferably with comparable spatial resolution, more tightly constrain estimates of molecular gas density and temperature in external galaxies than do observations solely of the corresponding ^{12}CO lines.

The rotational lines of CO are more useful, in general, for determining the physical conditions over the bulk of the molecular gas than other molecules because CO is abundant and its small dipole moment makes its lowest rotational transitions relatively easy to excite. Comparison of the strengths of different CO lines provides an estimate of the excitation because a higher-J transition of CO requires a higher gas density to thermalize and its intensity varies more rapidly with temperature than does a low-J transition. Molecular hydrogen itself is not a good probe of physical conditions because the bulk of the molecular gas is too cold (10–50 K) to excite the widely spaced rotational levels and because dipole transitions are forbidden.

The lines of ^{13}CO are more sensitive to density and temperature than the corresponding ^{12}CO lines, as the lower opacities in the ^{13}CO lines make it possible for the emission to better reflect the excitation differences and because radiative

[1] Work carried out at The University of Texas at Austin.

[2] CODE 685, NASA Goddard Space Flight Center, Greenbelt, MD 20771.
[3] Astronomy Department, The University of Texas at Austin, Austin, TX 78712-1083.
[4] Sterrewacht, Postbus 9513, 2300RA, Leiden, Netherlands.
[5] JILA, Campus Box 440, University of Colorado, Boulder, CO 80309.
[6] Joint Astronomy Centre, 665 Komohana Street, Hilo, HI 96720.

trapping effects do not as readily suppress non-LTE excitation in ^{13}CO. The ^{13}CO lines also probe more deeply into the molecular clouds. The greater sensitivity of the ^{13}CO lines can be illustrated by considering the ratio of the $J = 3 \rightarrow 2$ line strength to that of the $J = 2 \rightarrow 1$ line for both ^{13}CO and ^{12}CO. We abbreviate the ratios of the integrated radiation temperatures of the two lines by $^{13}R_{32}$ and $^{12}R_{32}$ {i.e., $^{x}R_{J\uparrow J\downarrow} \equiv \int T_{MB}[^{x}CO \quad J^{\uparrow} \rightarrow (J^{\uparrow} - 1)]dV / \int T_{MB}[^{x}CO \quad J^{\downarrow} \rightarrow (J^{\downarrow} - 1)]dV$, where T_{MB} is the main-beam radiation temperature}, respectively. Consider a molecular cloud with a kinetic temperature, T_K, of 30 K, a density, $n(H_2)$, of 10^7 cm^{-3} and a column density, $N(H_2)$, of 10^{22} cm^{-2} (for a velocity width of 10 km s^{-1}). The three lowest CO rotational levels in this cloud are thermalized, optically thick for ^{12}CO, and optically thin for ^{13}CO. *If we vary* T_K *between* 10 *and* 50 K, *we find that* $^{13}R_{32}$ *varies between* 0.5 *and* 1.6, *but* $^{12}R_{32}$ *only varies between* 0.7 *and* 0.9. *If we now fix* T_K *at* 30 K *and vary* $n(H_2)$ *between* 10^7 *and* 10^2 cm^{-3}, $^{13}R_{32}$ *will vary by an order of magnitude, whereas* $^{12}R_{32}$ *varies by a factor* $\lesssim 2$. In general, $^{13}R_{32}$ can reach 2.25 in the high temperature, optically thin limit, but $^{12}R_{32}$ cannot exceed $\simeq 1$ as long as the ^{12}CO lines are optically thick. (Of course, if the ^{13}CO lines are optically thick in a particular case, then $^{13}R_{32}$ will also be $\lesssim 1$.)

Information about the structure and physical conditions in the molecular interstellar medium in galaxies is very difficult to obtain. Individual clouds and the scale length for absorption of the exciting radiation are small compared to the typical linear resolution of molecular line observations. The region within a single beam is usually very heterogeneous since the various CO lines sample, with varying weights, the whole range of molecular material. Use of single-line indicators for mass, deposited energy, temperature, or density is therefore problematic. Use of multiple lines is more informative, but one must always be aware of the heterogeneous nature of the cloud population being studied.

Since we are interested in star formation, the densest portions of the molecular clouds in the inner regions of galaxies are of particular interest. In galactic clouds, the dense cores appear to account for the vast majority of current star formation (Lada 1992; Solomon, Downes, & Radford 1992). Higher J lines of rare CO isotopes, like ^{13}CO $J = 3 \rightarrow 2$, may arise primarily in these dense, star-forming cores and can provide information about the amount of such material. Low-lying transitions of less-abundant molecules with large dipole moments also arise in at least some of this denser gas. Observations of CS, NH_3, HCN, HC_3N, and other molecules can provide valuable additional information about temperatures and densities in this dense material (Mauersberger et al. 1989; Martin & Ho 1986; Nguyen-Q-Rieu, Nakai, & Jackson 1989; Mauersberger & Henkel 1990; Israel 1992).

In this paper, we use beam-matched observations of the $J = 3 \rightarrow 2$ and $J = 2 \rightarrow 1$ lines of ^{13}CO and ^{12}CO in a small sample of external galaxies to place limits on the molecular gas physical conditions in the central 500–1600 pc diameter of spiral galaxies. Unlike previous studies, which lacked the density- and temperature-sensitive ^{13}CO $J = 3 \rightarrow 2$ data (except Tilanus et al. 1991 for M82), we have detections of the ^{13}CO $J = 3 \rightarrow 2$ line in five external galaxies. In assessing physical conditions, we also place our data in the context of other published results on CO lines and lines from the high dipole moment molecules. The data also allow comparisons of the star formation rates per unit mass in the central few hundred parsecs with those in the outer star-forming disks of spiral galaxies. We include data from observations of IC 342, NGC 253, and M83 (Wall & Jaffe 1990; Wall et al. 1991; Wall 1991) as well as new $J = 3 \rightarrow 2$ ^{13}CO and ^{12}CO data for NGC 6946 and $J = 3 \rightarrow 2$, $J = 2 \rightarrow 1$ ^{13}CO and ^{12}CO data for Maffei 2, and $C^{18}O$ and ^{13}CO $J = 1 \rightarrow 0$ data for NGC 253 and M82. We chose this particular sample of galaxies because they are nearby ($\sim$2–5 Mpc), infrared-bright ($L_{IR} \sim 10^9$–10^{10} $L_{\odot}$; Telesco & Harper 1980; Becklin et al. 1980; *IRAS* Point Source Catalog 1985), and are bright in the ^{12}CO $J = 1 \rightarrow 0$ line (e.g., Rickard et al. 1977a, b; Young & Scoville 1982b).

2. OBSERVATIONS

The ^{13}CO and ^{12}CO $J = 2 \rightarrow 1$ and $J = 3 \rightarrow 2$ lines were observed in the galaxies NGC 253, M83, IC 342, Maffei 2, and NGC 6946 during 1988–1991. Tables 1 and 2 summarize the line frequencies and details of the observations. The $J = 3 \rightarrow 2$ and $J = 2 \rightarrow 1$ observations had $\sim 20''$ (FWHM) beam sizes and main-beam efficiencies, η_{MB}, of 0.5–0.6. The $J = 1 \rightarrow 0$ lines of $C^{18}O$ and ^{13}CO were observed in 1991 with a $55''$ beam. For all observations, the pointing accuracy was better than $\frac{1}{4}$ to $\frac{1}{3}$ of a beam width. The line intensities were calibrated in units of main-beam radiation temperature, T_{MB}, which is the radiation temperature of a uniform source filling the beam to the first null. Our observations were calibrated by observations of Mars and Jupiter (Wright 1976; Hildebrand et al. 1985). The estimated uncertainty of the line ratios is $\pm 30\%$. When observing the 331 GHz ^{13}CO $J = 3 \rightarrow 2$ line, a strong telluric H_2O line near 325 GHz causes the atmospheric opacity in the signal and image sidebands to differ. Atmospheric modeling shows that, for our lower sideband observations with $\nu_{IF} = 1.4$ GHz, the correction to the standard chopper wheel calibration is $\lesssim 10\%$ under the dry conditions found at the summit of Mauna Kea (i.e., < 2 mm of precipitable water vapor). We have not applied such a correction.

3. RESULTS

In this section, we describe the observed line ratios and apply LTE analysis to set temperature limits on the emitting molecular gas. Consistency or inconsistency of the line strengths with the LTE ratios can indicate, in some cases, whether the gas density is higher or lower than the critical density of the $J = 3 \rightarrow 2$ line [$n(H_2) \simeq 5 \times 10^4$ cm^{-3}]. Indeed, throughout this paper we dub "high"-density gas as $n(H_2) \gtrsim 10^4$ cm^{-3} and "low"-density gas as $n(H_2) \lesssim 10^4$ cm^{-3}. (Because 10^4 cm^{-3} is a generous upper limit for "low"-density molecular gas, LVG modeling often suggests even lower densities; see § 4.1.2, for example.) Table 3 shows the adopted parameters for each galaxy. Tables 4 and 5 describe the new data. Figures 1, 2, 3, and 4 show the spectra for M83, NGC

TABLE 1

FREQUENCIES OF OBSERVED LINES

Line	Frequency (GHz)
$C^{18}O$ $J = 1 \rightarrow 0$.....	109.782
^{13}CO $J = 1 \rightarrow 0$.....	110.201
^{13}CO $J = 2 \rightarrow 1$.....	220.399
^{12}CO $J = 2 \rightarrow 1$.....	230.538
^{13}CO $J = 3 \rightarrow 2$.....	330.588
^{12}CO $J = 3 \rightarrow 2$.....	345.796

TABLE 2

OBSERVATIONS

Galaxy	Line	Beam Size FWHM (±2″)	η_{MB}	Number of Points	Telescope	Date
NGC 253[a]	^{13}CO (3 → 2)	22″	0.5	5	CSO[b] 10 m	1989 Nov 7
	^{12}CO (3 → 2)	22	0.5	11	CSO 10 m	1989 Jun 12
	^{13}CO (2 → 1)	24	0.5	7	SEST[c] 15 m	1989 Jul 1–12
	^{12}CO (2 → 1)	24	0.5	14	SEST 15 m	1989 Jul 1–12
	^{13}CO (2 → 1)	21	0.6	1	JCMT[d] 15 m	1988 Aug 9–10
	^{12}CO (2 → 1)	21	0.6	5	JCMT 15 m	1988 Aug 9–10
	^{13}CO (1 → 0)	55	0.8	1	NRAO[e] 12 m	1991 Mar 18
	C^{18}O (1 → 0)	55	0.8	1	NRAO 12 m	1991 Mar 18
IC 342[f]	^{13}CO (3 → 2)	22	0.5	1	CSO 10 m	1989 Nov 7
	^{12}CO (3 → 2)	15	0.6	7	JCMT 15 m	1988 Aug 10
M83[g]	^{13}CO (3 → 2)	22	0.5	3	CSO 10 m	1990 Apr 3–7
	^{12}CO (3 → 2)	22	0.5	8	CSO 10 m	1990 Apr 3–7
	^{13}CO (2 → 1)	22	0.6	2	JCMT 15 m	1989 Feb 20
	^{12}CO (2 → 1)	22	0.6	43	JCMT 15 m	1989 Feb 16–20
						1989 Jun 7–8
						1990 Jan 13
Maffei 2	^{13}CO (3 → 2)	22	0.5	1	CSO 10 m	1990 Jul 24
	^{12}CO (3 → 2)	22	0.5	4	CSO 10 m	1989 Nov 3
	^{13}CO (2 → 1)	21	0.6	1	JCMT 15 m	1988 Aug 9
	^{12}CO (2 → 1)	21	0.6	5	JCMT 15 m	1988 Aug 9
NGC 6946	^{13}CO (3 → 2)	22	0.5	1	CSO 10 m	1990 Jul 23
	^{12}CO (3 → 2)	22	0.5	6	CSO 10 m	1989 Apr 19
M82	^{13}CO (1 → 0)	55	0.8	1	NRAO 12 m	1991 Mar 18
	C^{18}O (1 → 0)	55	0.8	1	NRAO 12 m	1991 Mar 18

[a] Wall et al. 1991 for $J = 3 \rightarrow 2$ and $J = 2 \rightarrow 1$ lines.
[b] Caltech Submillimeter Observatory, Mauna Kea, HI.
[c] Swedish ESO Submillimeter Telescope, La Silla, Chile.
[d] James Clerk Maxwell Telescope, Mauna Kea, HI.
[e] National Radio Astronomy Observatory, Kitt Peak, AZ.
[f] Wall & Jaffe 1990.
[g] Wall et al. 1991.

6946, and Maffei 2. IC 342, NGC 253, and M83 are discussed in more detail elsewhere (Wall & Jaffe 1990; Wall 1991; Wall et al. 1991).

The ratio of the $J = 3 \rightarrow 2$ to $J = 2 \rightarrow 1$ line strengths in ^{12}CO and ^{13}CO peak near the center of each galaxy, except for IC 342. Incomplete mapping of the ^{13}CO $J = 3 \rightarrow 2$ line indicates that the ratio of ^{13}CO $J = 3 \rightarrow 2$ to ^{13}CO $J = 2 \rightarrow 1$ line strength peaks at the centers of NGC 253 and M83. The corresponding ratio for the ^{12}CO lines, $^{12}R_{32}$, shows evidence of simple decline from a single peak (with 10″ of the center) in NGC 253, M83, and Maffei 2, but no particular spatial trend in IC 342. We did not take ^{12}CO $J = 2 \rightarrow 1$ data toward NGC 6946, so we have used the 17″ resolution ^{12}CO $J = 1 \rightarrow 0$ data of Sofue et al. (1988) to compute $^{12}R_{31}$ ratios (see Table 5). Disregarding position (−18″, −9″), where the ^{12}CO $J = 1 \rightarrow 0$ spectrum has a low signal-to-noise ratio, the $^{12}R_{31}$ values in NGC 6946 peak at position (9″, 9″) and show a rapid decline at the northern position (9″, 18″) and a more gradual decline in other directions.

TABLE 3

ADOPTED PARAMETERS

Galaxy	α(1950)	δ(1950)	D (Mpc)	Beam[a] (pc)	i
NGC 253[b]	0^{h}45^m 5^s.8	−25°33′38″	2.5	240	78°.5
IC 342[c]	3 41 57.0	67 56 29	1.8	170	25°
M83	13 34 11.3[d]	−29 36 39[d]	3.7[e]	360	24°[f]
Maffei 2[g]	2 38 8.5	59 23 24	5	480	60°
NGC 6946[g]	20 33 48.8	59 58 50	5.5[h]	530	30°
M82[i]	9 51 43.9	69 55 1	3.3	320	82°

[a] 20″ on galaxy.
[b] See Wall et al. 1991 for references.
[c] See Wall & Jaffe 1990 for references.
[d] *IRAS* Point Source Catalog.
[e] de Vaucouleurs 1979.
[f] Talbot et al. 1979.
[g] See Weliachew, Casoli, & Combes 1988 for references.
[h] Tully 1988.
[i] See Olofsson & Rydbeck 1984 for references.

Table 6 lists the $^{13}R_{32}$ and $^{12}R_{32}$ values for the central 20″ diameter regions in the galaxies in our sample. Table 6 also lists the minimum T_K allowed for the observed $^{12}R_{32}$ averaged over the central 20″ and 60″ diameters (the 60″ average excludes the central 20″ diameter). Each T_K was calculated for LTE conditions in the optically thick and optically thin limits; the smaller of the two possible T_K values appear in Table 6. Because the optically thin value of T_K was the smaller value for our galaxies (except for IC 342), the computed kinetic temperatures are lower limits since nonnegligible optical depths would increase the estimated kinetic temperatures. In addition, the assumption of LTE underestimates T_K values, since non-LTE conditions require higher T_K for a given $^{12}R_{32}$. The minimum kinetic temperatures in Table 6 are 14–30 K in the central 20″ and 11–18 K in the central 60″; even allowing for 30% uncertainties in the line ratios the minimum kinetic temperatures would be 12–18 K and 10–13 K, respectively (except

TABLE 4

MAFFEI 2 LINE PARAMETERS

POSITION Δα″, Δδ″	T_{MB} (Peak) (K)	$\int T_{MB}\,dV$ (K km s^{-1})	V_{peak} (km s^{-1})	V_{mean} (km s^{-1})	$\Delta V_{(FWHM)}$ (km s^{-1})
		^{12}CO $J = 3 \rightarrow 2$			
5, 15	1.1	90	−80	−75	65
0, 6	1.5	240	−65	−45	130
−5, −3	1.5	200	0	−15	135
−10, −12	1.5	120	15	15	90
		^{12}CO $J = 2 \rightarrow 1$			
10, 18	0.9	115	−55	−25	120
5, 9	1.8	150	−75	−80	70
0, 0	1.8	190	−70	−70	80
−5, −9	1.7	205	10	−5	80
−10, −18[a]	∼1.8	∼160	15	10	80
		^{13}CO $J = 3 \rightarrow 2$			
0, 0	0.29	40	−85	−75	120
		^{13}CO $J = 2 \rightarrow 1$			
0, 0	∼0.12	∼25	...	−35	220

[a] The faulty baseline for this spectrum renders the parameters here untrustworthy.

TABLE 5

NGC 6946 LINE PARAMETERS

POSITION Δα″, Δδ″	T_{MB} (Peak) (K)	$\int T_{MB}\,dV$ (K km s^{-1})	V_{peak} (km s^{-1})	V_{mean} (km s^{-1})	$\Delta V_{(FWHM)}$ (km s^{-1})	$^{12}R_{31}$[a]
			^{12}CO $J = 3 \rightarrow 2$			
18, 9.	0.74	40	−20	−5	30	0.98
9, 18.	0.97	75	−15	10	50	0.47
9, 9.	1.4	160	−15	30	135	1.7
0, 0.	1.4	200	90	70	160	1.3
−9, −18.	0.46	50	115	95	60	0.65
−18, −9.	0.4	30	120	115	60	2.5
			^{13}CO $J = 3 \rightarrow 2$			
0, 0.	∼0.18	∼28	∼20	∼25	∼200	

[a] Ratio of $J = 3 \rightarrow 2$ to $J = 1 \rightarrow 0$ integrated radiation temperatures for ^{12}CO, using the ^{12}CO $J = 1 \rightarrow 0$ data of Sofue et al. 1988.

for IC 342, which is probably subthermally excited in the CO $J = 2 \rightarrow 1$ and $J = 3 \rightarrow 2$ lines anyway, see Wall & Jaffe 1990). Therefore the central 60″ (500–1600 pc) diameter regions contain molecular gas that is at least as warm as that in our Galaxy (i.e., $T_K \simeq 5$–20 K, Sanders et al. 1985, Dickman et al. 1975) and possibly warmer. Also, the $^{12}R_{32}$ values in Table 6 suggest that the central 20″ (170–530 pc) regions contain even warmer molecular gas than the surrounding region (except in IC 342). The detection of the CO $J = 4 \rightarrow 3$ and $J = 6 \rightarrow 5$ lines in some of these galaxies provides further qualitative evidence for the existence of at least some warm gas in the inner regions (Güsten et al. 1993; Harris et al. 1991).

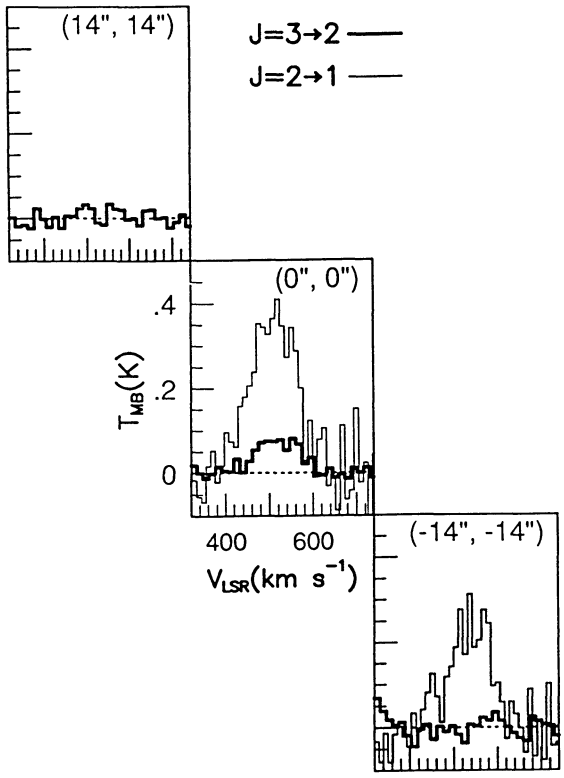

FIG. 1.—The ^{13}CO $J = 3 \rightarrow 2$ and ^{13}CO $J = 2 \rightarrow 1$ spectra along the major axis of M83 are illustrated as T_{MB} vs. V_{LSR}. $^{13}R_{32}$ is 0.2 at (0″, 0″) and <0.1 at (−14″, −14″).

3.1. *Central* 20″

The observed line ratios, particularly $^{13}R_{32}$, imply that the physical conditions of the molecular gas in the central 20″ (170–530 pc) diameter vary strongly from galaxy to galaxy. The $^{12}R_{32}$ values vary from 0.4 to 1.3. The $^{13}R_{32}$ values range from 0.2 to 2.0 (see Fig. 1 and Wall et al. 1991) and show no correlation with the corresponding $^{12}R_{32}$. For instance, in NGC 253, M82, and Maffei 2, where $^{12}R_{32} = 1.1$–1.3, $^{13}R_{32}$ ranges from 0.2 (in M83) to 2.0 (in NGC 253). The values of $^{12}R_{32}$ require warm ($T_K > 20$ K) molecular gas in each of these three galaxies; as we will show in the non–LTE analysis in § 4.1.1, the range in $^{13}R_{32}$ values reflects a large difference in molecular gas densities [i.e., $n(H_2) \lesssim 10^3$ cm^{-3} in M83, $n(H_2) \gtrsim 10^5$ cm^{-3} in NGC 253]. In IC 342, the observed $^{13}R_{32}$, along with C^{18}O observations, indicate optically thick ^{13}CO emission (Wall & Jaffe 1990).

3.2. *Central* 60″

$^{13}R_{32}$ is small (i.e., $^{13}R_{32} \lesssim 0.1$) for those positions observed outside the central 20″ diameter regions. $^{13}R_{32}$ declines with increasing galactocentric radius in both M83 and NGC 253. Figure 1 shows that in M83, at positions 20″ northeast and southwest of the center, the ^{13}CO $J = 3 \rightarrow 2$ line strengths are $T_{MB} \leq 0.04$ K, which suggests low $^{13}R_{32}$ values at these positions (indeed, $^{13}R_{32} < 0.1$ at 20″ southwest). In NGC 253, the pointlike ^{13}CO $J = 3 \rightarrow 2$ emission implies a very small $^{13}R_{32}$ (<0.1) outside the nucleus.

A lower $^{13}R_{32}$ away from the center implies that molecular gas densities are lower [i.e. $n(H_2) \lesssim n_{crit}(J = 3 \rightarrow 2) \simeq 5 \times 10^4$ cm^{-3}] at these positions. An alternative explanation for low $^{13}R_{32}$ is low kinetic temperature, T_K. The observed $^{13}R_{32}$ is so small, however ($^{13}R_{32} \leq 0.1$), that even for molecular clouds similar to those in the first Galactic quadrant (i.e., most

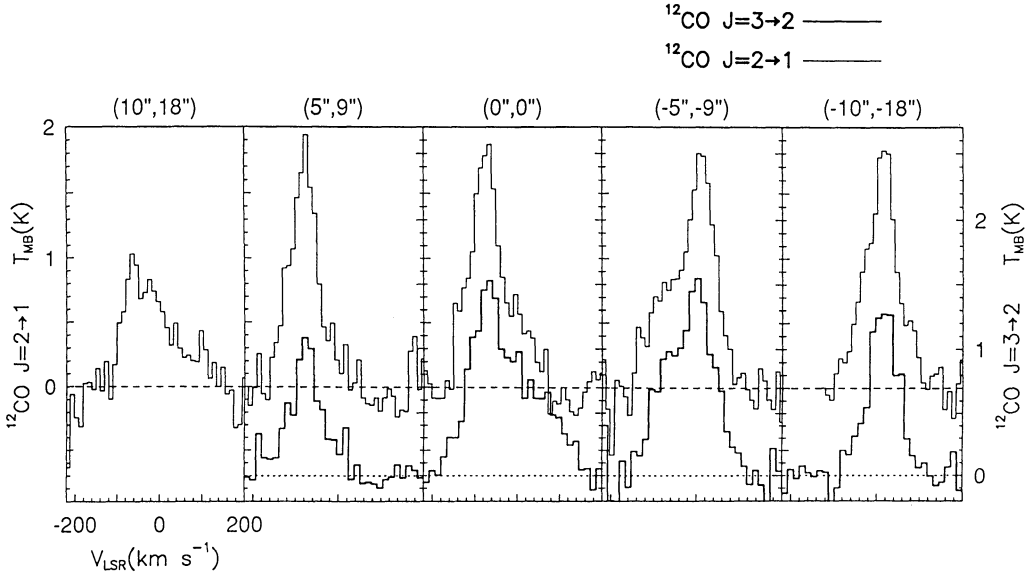

FIG. 2.—The ^{12}CO $J = 3 \rightarrow 2$ and ^{12}CO $J = 2 \rightarrow 1$ spectra along the major axis of Maffei 2 are shown as main beam radiation temperature, T_{MB}, vs. LSR velocity, V_{LSR}. The vertical scales for the $J = 3 \rightarrow 2$ and $J = 2 \rightarrow 1$ spectra have been offset for clarity. The ^{12}CO $J = 2 \rightarrow 1$ spectrum at $(-10'', -18'')$ should be viewed with caution since the baseline problems made it necessary to truncate the spectrum for $V_{LSR} < -120$ km s^{-1}. The ^{12}CO $J = 3 \rightarrow 2$ spectra are within 6″ of the indicated positions.

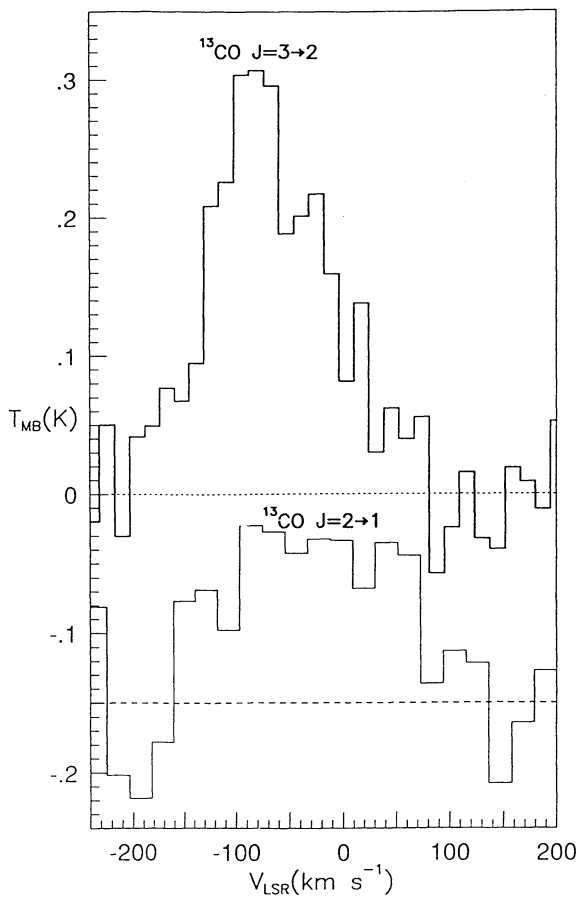

FIG. 3.—The ^{13}CO $J = 2 \rightarrow 1$ and ^{13}CO $J = 3 \rightarrow 2$ spectra of Maffei 2 at, or within 6″ of, (0, 0) are displayed as T_{MB} vs. V_{LSR}. The $J = 2 \rightarrow 1$ spectrum has been offset vertically from the $J = 3 \rightarrow 2$ spectrum for clarity.

warmer than 6 K; Sanders et al. 1985), the T_K implied by $^{13}R_{32}$ assuming the LTE limit would be lower than the kinetic temperature. While kinetic temperatures lower than those in the central 20″ diameter are not ruled out, lower densities are required for clouds outside the inner 20″ diameter to explain the low $^{13}R_{32}$.

The $J = 1 \rightarrow 0$ C^{18}O and ^{13}CO data imply appreciable opacity in the ^{13}CO $J = 1 \rightarrow 0$ line over the central 60″ (i.e., 720 pc) diameter of NGC 253 (see Fig. 5). It is usually assumed that the ^{13}CO lines are optically thin because they are ~5–10 times weaker than their ^{12}CO counterparts. However, the true ^{13}CO line optical depth is underestimated if the ^{13}CO line has a lower excitation temperature than the corresponding ^{12}CO line or if nonuniformities lead to regions within the beam with higher ^{13}CO opacities while preserving the globally high ^{12}CO/^{13}CO ratio. The ^{13}CO $J = 1 \rightarrow 0$ to C^{18}O $J = 1 \rightarrow 0$ intensity ratio provides another way to estimate the ^{13}CO $J = 1 \rightarrow 0$ line optical depth. For example, if this ratio is less than ~60% of the ^{13}CO/C^{18}O abundance ratio, the ^{13}CO $J = 1 \rightarrow 0$ line is appreciably saturated (i.e., $\tau \gtrsim 1$). In NGC 253, the ratio of the ^{13}CO $J = 1 \rightarrow 0$ integrated radiation temperature to that of the C^{18}O $J = 1 \rightarrow 0$ line is 3.1 ± 0.9, the same as that in Sgr B2 (Lis & Goldsmith 1989). The ^{13}CO/C^{18}O abundance ratio in our Galaxy ranges from 5.5 to 9.0 (Wannier 1989), resulting in $\tau(^{13}\text{CO}\ J = 1 \rightarrow 0) \sim 1$–5 if abundances are similar in NGC 253 and we assume that the excitation temperatures are the same for the $J = 1 \rightarrow 0$ lines of both ^{13}CO and C^{18}O. This compares with the value $\tau(^{13}\text{3O}\ J = 1 \rightarrow 0) \sim 1$–3 in the central 20″ (170 pc) of IC 342 (Eckart et al. 1990; Wall & Jaffe 1990). The high ^{13}CO $J = 1 \rightarrow 0$ optical depth in NGC 253 implies that the molecular clouds dominating the $J = 1 \rightarrow 0$ emission of ^{13}CO and C^{18}O have column densities of $\gtrsim 7 \times 10^{22}$ cm^{-2} or $A_v \gtrsim 50$ mag for $\Delta V_{cloud} = 10$ km s^{-1} (and assuming a standard Galactic dust-to-gas ratio). M82 (see Fig. 6) has a ^{13}CO/C^{18}O integrated radiation temperature ratio of 4.6 ± 1.4, consistent with any

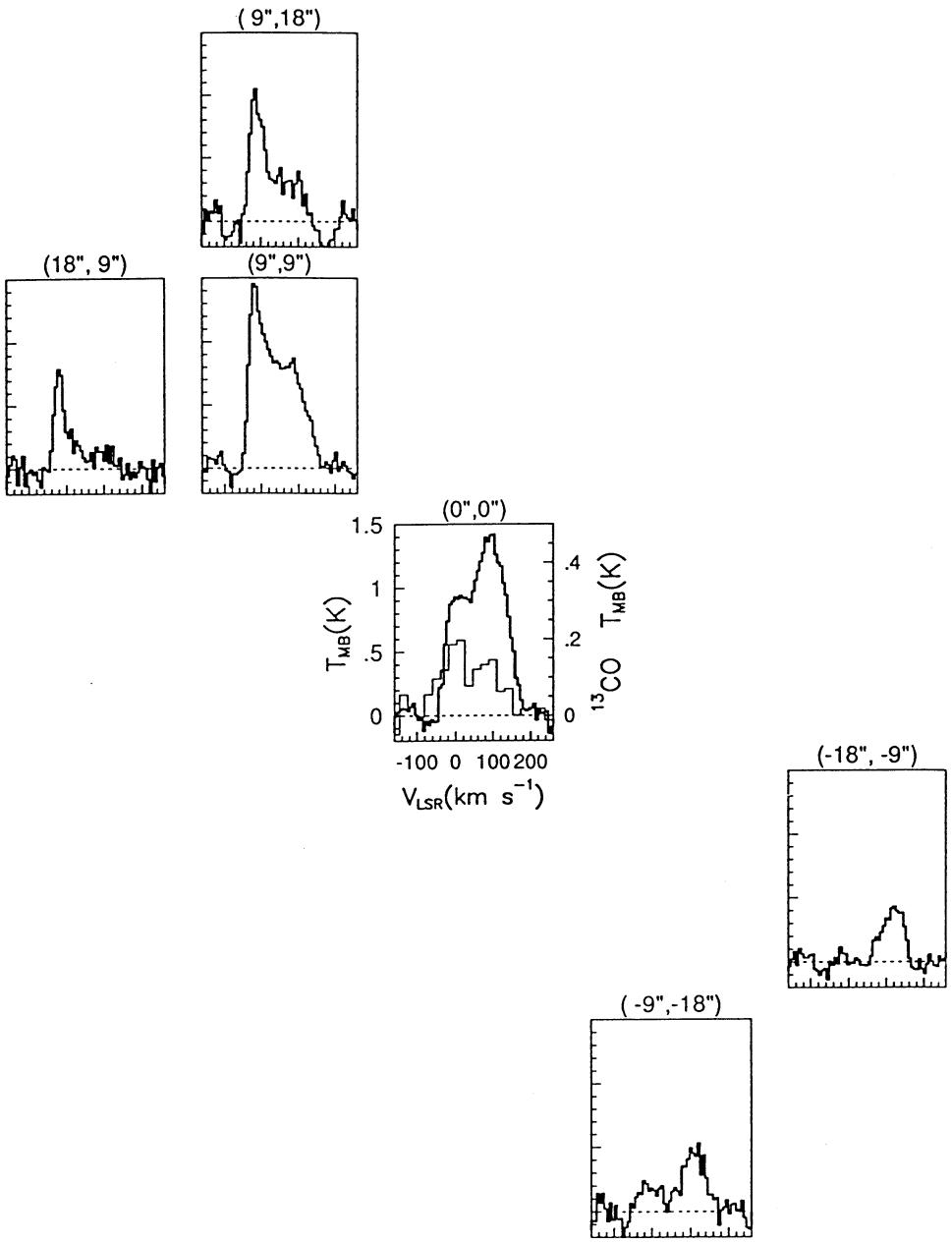

FIG. 4.—The ^{12}CO $J = 3 \rightarrow 2$ spectra (in thick lines) toward six positions in NGC 6946 are illustrated. Also shown at (0, 0) is a ^{13}CO $J = 3 \rightarrow 2$ spectrum (in thin line and with different T_{MB} scale).

^{13}CO $J = 1 \rightarrow 0$ optical depth $\lesssim 3$ (again assuming LTE). For sufficiently low densities [i.e., $n(H_2) \lesssim 10^3$ cm^{-3} for the $J = 1 \rightarrow 0$ line], the ^{13}CO $J = 1 \rightarrow 0$ optical depths given above are underestimates. If some of the clouds are optically thin in the rare-isotope CO line emission, then the global intensity ratios underestimate the ^{13}CO opacity of the bulk of the material. Factors affecting the ^{13}CO/C^{18}O abundance ratio are also likely to result in $\tau(^{13}\text{CO } J = 1 \rightarrow 0)$ being higher than our estimates. Chemical fractionation effects, for instance, increase the ^{13}CO/C^{18}O abundance ratio (van Dishoeck & Black 1988). Similarly, the ^{13}CO/C^{18}O abundance ratio in red giants can range from the solar value (i.e., 5.5) to an order of magnitude higher (Wannier 1989). A recent suggestion that the C^{18}O abundance may be high in starburst galaxies (Sage, Mauersberger, & Henkel 1991) is not inconsistent with optically thick ^{13}CO $J = 1 \rightarrow 0$ and ^{13}CO $J = 2 \rightarrow 1$ if the ^{13}CO/C^{18}O abundance ratio is the same as the Galactic value (i.e., 5–9; Wannier 1989). In IC 342, additional evidence for a high ^{13}CO line opacity comes from measurements of $^{13}R_{21}$ and $^{13}R_{32}$ (Wall & Jaffe 1990; Eckart et al. 1990). It is quite likely, therefore, that ^{13}CO $J = 1 \rightarrow 0$ optical depths ≥ 1 are common, even over 10^2–10^3 pc scales, in some of the galaxies we have studied.

The mass of H_2, $M(H_2)$, within the central 1′ (500–1600 pc) diameter of each galaxy is given in Table 7. Also listed are the $M(H_2)$ values derived from the observations of others (e.g., Young & Scoville 1982b), and atomic gas masses, M(H I), and dynamical masses, M_{dyn}, culled from the literature. Our $M(H_2)$

TABLE 6

LINE RATIOS

Galaxy	$^{13}R_{32}(20'')^a$	$^{12}R_{32}(20'')^a$	Minimum $T_K(20'')^b$ (K)	$^{12}R_{32}(60'')^c$	Minimum $T_K(60'')^c$ (K)
NGC 253	2.0	1.1	23	0.9	18
IC 342.....	1.0	0.4[d]	4	0.5	7
M83	0.2	1.1	23	0.9	18
Maffei 2	1.6	1.3	30	0.9	18
NGC 6946	...	1.3[e]	14	0.9[e]	11

[a] Averaged over central 20″ diameter.
[b] Estimated from $^{12}R_{32}$ only (e.g., $^{13}R_{32}$ implies $T_K \gtrsim 50$ K for both NGC 253 and Maffei 2).
[c] Averaged over central 60″ diameter, excluding central 20″ diameter.
[d] Averaged over central 15″ diameter.
[e] This is actually $^{12}R_{31}$ from the ^{12}CO $J = 1 \rightarrow 0$ data of Sofue et al. 1988.

estimates represent lower limits to the molecular gas mass because we use column densities derived from ^{13}CO integrated line strengths assuming that these lines are optically thin. The positions observed in ^{13}CO did not cover the central 1′ diameter (except in NGC 253), so we obtained an average $N(H_2)$-to-$\int T_{MB}(^{12}CO\ J = 2 \rightarrow 1)dV$ ratio, for those positions where ^{13}CO lines were observed, and multiplied this ratio by the $\int T_{MB}(^{12}CO\ J = 2 \rightarrow 1)dV$ averaged over the central 1′ diameter of each galaxy. In NGC 6946, both $N(H_2)$-to-$\int T_{MB}(^{12}CO\ J = 1 \rightarrow 0)dV$ and $N(H_2)$-to-$\int T_{MB}(^{12}CO\ J = 3 \rightarrow 2)dV$ ratios were used and yielded nearly identical $M(H_2)$s. In M82, the ^{13}CO $J = 2 \rightarrow 1$ and ^{12}CO $J = 2 \rightarrow 1$ data of Loiseau et al. (1990) were used. The ^{13}CO column densities assumed the kinetic temperatures given by $^{13}R_{32}$ or $^{12}R_{32}$ values (i.e., $T_K = 20$–50 K; but see Wall et al. 1991 for NGC 253), and in M82, $T_K = 35$ K was adopted from Tilanus et al. (1991). The resultant $M(H_2)$ values used a ^{13}CO/^{12}CO

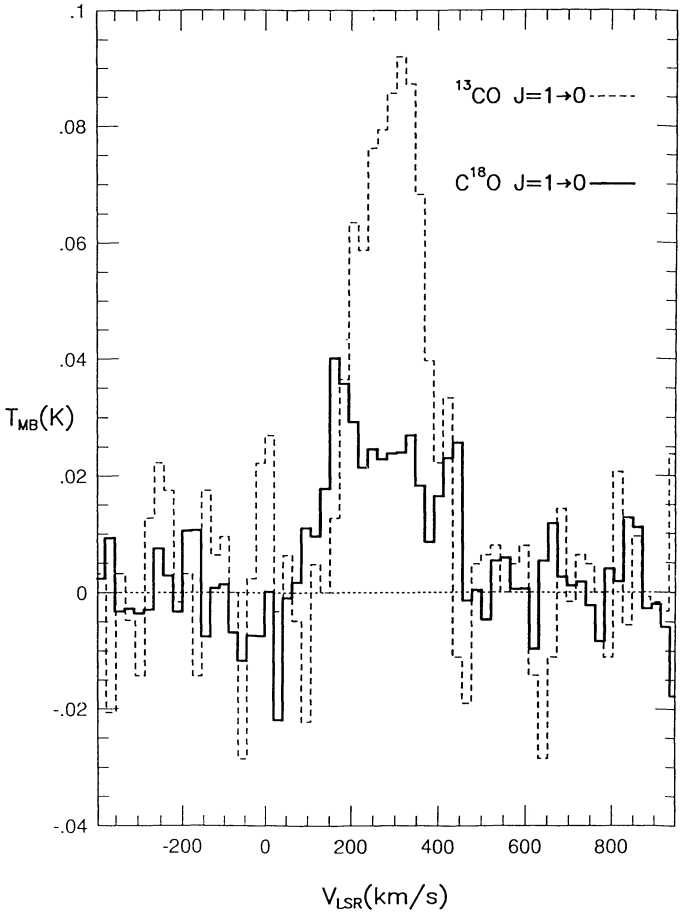

FIG. 5.—The $J = 1 \rightarrow 0$ lines of $C^{18}O$ and ^{13}CO were observed toward NGC 253 in a 55″ beam. The $C^{18}O$ $J = 1 \rightarrow 0$ spectrum in the figure has a parabolic baseline removed, which has increased the integrated intensity by 60%. Even without the removed baseline, the ratio of ^{13}CO $J = 1 \rightarrow 0$ to $C^{18}O$ $J = 1 \rightarrow 0$ integrated intensities is as low as 3.1.

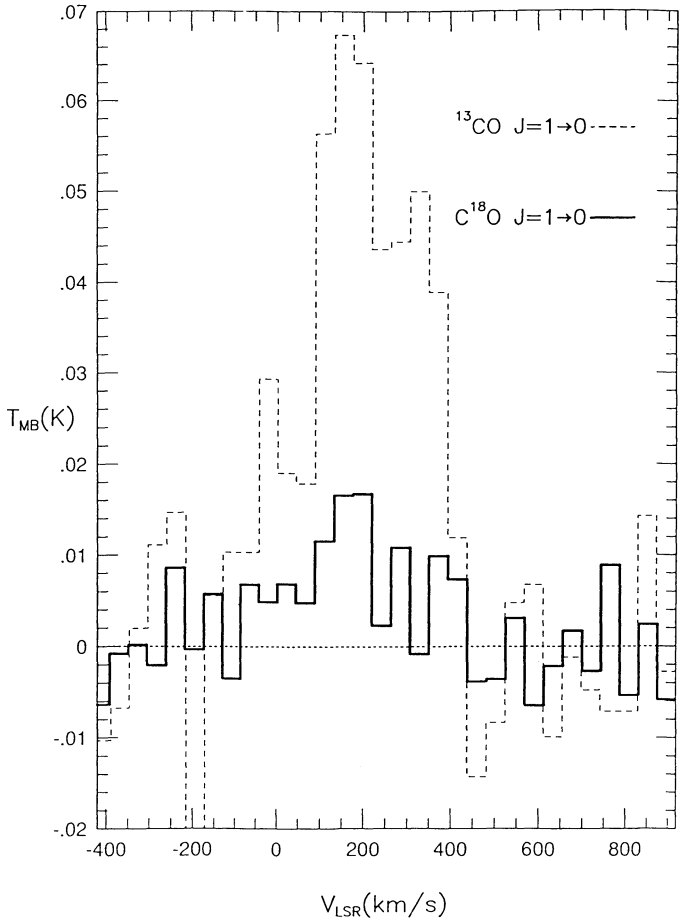

FIG. 6.—A marginal detection of the $C^{18}O$ $J = 1 \rightarrow 0$ line in M82 is shown along with a ^{13}CO $J = 1 \rightarrow 0$ spectrum, both observed in 55″ beams. The ratio of the ^{13}CO $J = 1 \rightarrow 0$ to $C^{18}O$ $J = 1 \rightarrow 0$ integrated intensities is 4.6.

TABLE 7

MASS IN THE CENTRAL 1′ DIAMETER

GALAXY	$M(H_2)(M_\odot)$ ^{13}CO[a]	$M(H_2)(M_\odot)$ ^{12}CO[b]	M(H I) ($M_\odot$)	M_{dyn} ($M_\odot$)	$[M(H_2)^c + M(H\ I)]/M_{dyn}$
NGC 253	4×10^7	1×10^{8}[d]	1×10^{7}[e]	2×10^{9}[d]	0.03
IC 342	7×10^6	3×10^{7}[f]	2×10^{5}[g]	3×10^{8}[g]	0.1
M83	7×10^7	1×10^{8}[f]	6×10^{6}[h]	10^{9}[i]	0.08
Maffei 2	7×10^7	4×10^{8}[j]	1×10^{7}[k]	1.4×10^{9}[l]	0.06
NGC 6946	6×10^7	4×10^{8}[f]	2×10^{7}[m]	1.3×10^{9}[m]	0.06
M82	8×10^7	4×10^{8}[n]	2×10^{7}[p]	1.4×10^{9}[q]	0.07

[a] Using ^{13}CO derived column densities to determine an integrated $T_{MB}(^{12}CO)$ to H_2 column density conversion factor.
[b] Using standard integrated $T_{MB}(^{12}CO)$ to H_2 column density conversion factor [i.e., 4×10^{20} cm^{-2} (K km s^{-1})$^{-1}$].
[c] Using $M(H_2)$ from this work.
[d] Scoville et al. 1985.
[e] Combes, Gottesman, & Weliachew 1977.
[f] Young & Scoville 1982b data and 4×10^{20} cm^{-2} (K km s^{-1})$^{-1}$ conversion factor at our distance.
[g] Newton 1980 adjusted to our distance.
[h] Rogstad, Lockhart, & Wright 1974 adjusted to our distance.
[i] Handa et al. 1990.
[j] Weliachew et al. 1988 data and 4×10^{20} cm^{-2} cm^{-2} (K km s^{-1})$^{-1}$ conversion factor.
[k] Wright & Seielstad 1973 data adjusted to our distance.
[l] Weliachew et al. 1988 velocities.
[m] Carignan et al. 1990 data.
[n] Young & Scoville 1984.
[p] Crutcher, Rogstad, & Chu 1978.
[q] Heckathorn 1972.

abundance ratio of 1/30, similar to that determined for the Galactic center (Langer & Penzias 1990) and similar to that inferred for the center of M82 (Tilanus et al. 1991), and used a $^{12}CO/H_2$ abundance of 1×10^{-4}. The values of $M(H_2)$ determined here are factors of 1–7 lower than derived in previous work. We find that the interstellar medium (ISM) accounts for 3%–10% of the total mass in the central 1′ of these galaxies. If ^{13}CO is optically thin, the standard conversion factor overestimates the central masses a factor of ~ 3.

4. DISCUSSION

4.1. *Molecular Gas Temperature and Density*

4.1.1. *Central 20″*

The different $^{13}R_{32}$ values observed in different galaxies represent real differences in molecular gas physical conditions and are not distance artifacts. For example, if NGC 253 were placed at the distance of M83, its nuclear $^{13}R_{32}$ would be 0.9 in our 20″ beam. Since $^{13}R_{32}$ in M83 is 0.2, the central 20″ of M83 is not simply a more distant version of NGC 253. On the other hand, it is possible that the $^{13}R_{32} = 2.0$ "hot spot" observed in NGC 253 is present in other galaxies, but its linear scale varies greatly from galaxy to galaxy. In NGC 253 the "hot spot" is $\lesssim 200$ pc across; such a "hot spot" in M83 cannot be more than ~ 100 pc across because of the low observed $^{13}R_{32}$. In this picture, the different $^{13}R_{32}$ values would simply reflect the different-sized "hot spots" in different galactic nuclei. This picture is inconsistent, however, with the data for IC 342 because the ^{13}CO $J = 2 \rightarrow 1$ line is optically thick in that galaxy (Wall & Jaffe 1990), restricting $^{13}R_{32}$ to $\lesssim 1$.

The galaxy-to-galaxy variation of $^{13}R_{32}$ in the central 20″ (170–530 pc) diameters can be explained by varying the relative amounts of warm, high-density, and low-density molecular gas. To test the effects of density changes, the Large Velocity Gradient (LVG) models (see Goldreich & Kwan 1974 and de Jong, Chu, & Dalgarno 1975), which include non-LTE (low density and radiative trapping) effects, have been used. The LVG models use the collision rate coefficients of Flower & Launay (1985) for $T_K \leq 100$ K and Schinke et al. (1985) for $T_K > 100$ K. We find that mixing varying amounts of a high-density component, where $n(H_2) = 10^5$ cm^{-3}, with a low-density component, where $n(H_2) = 300$ cm^{-3}, both components having $T_K = 100$ K, can reproduce the observed $^{13}R_{32}$ and $^{12}R_{32}$ values to within $\pm 30\%$, except in IC 342. In IC 342 it is difficult to simultaneously match a low $^{12}R_{32}$ ($= 0.4$) with a $^{13}R_{32}$ as high as 1, unless the low-density component is colder ($T_K \sim 10$–20 K) and we allow the column densities to vary (see § 4.1.3).

The high $^{13}R_{32}$ observed in the central 20″ diameter of NGC 253 (see Wall et al. 1991) suggests optically thin ^{13}CO lines and may, at first glance, seem at odds with the high optical depth inferred for the ^{13}CO $J = 1 \rightarrow 0$ line from the ^{13}CO $J = 1 \rightarrow 0$/$C^{18}O$ $J = 1 \rightarrow 0$ intensity ratio. Nevertheless, no inconsistency exists between the $^{13}R_{32}$ and ^{13}CO $J = 1 \rightarrow 0/C^{18}O$ $J = 1 \rightarrow 0$ ratios because the $J = 1 \rightarrow 0$ observations apply to the entire central $\sim 60''$ diameter whereas the $^{13}R_{32}$ values applies to the central 20″ diameter. In addition, the spatial distribution of the ^{13}CO $J = 2 \rightarrow 1$ emission (see Wall et al. 1991) suggests that $\sim 80\%$ of the ^{13}CO emission originates outside the central 20″. Hence, the conclusion that the $J = 1 \rightarrow 0$ and $J = 2 \rightarrow 1$ lines may be optically thick outside the central 20″ region, but optically thin inside this region is not unreasonable—especially since the high kinetic temperature ($T_K \gtrsim 100$ K) inside the 20″ region would spread the molecules over a larger number of rotational levels.

4.1.2. *Central 60″*

Non–LTE calculations imply that most of the ^{13}CO emission from outside the inner 20″ diameter region arises in low-density gas. LVG models can help to set density constraints on

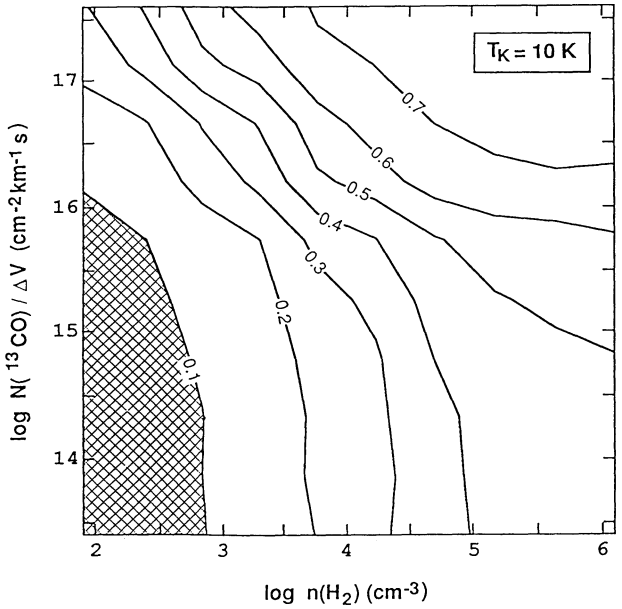

FIG. 7.—Contours of constant $^{13}R_{32}$ are plotted as functions of ^{13}CO column density per velocity interval, $N(^{13}\mathrm{CO})/\Delta V$, and molecular gas density, $n(\mathrm{H_2})$. The range of $N(^{13}\mathrm{CO})/\Delta V$ corresponds to $A_v \sim 0.1$–1000 mag for molecular clouds with velocity widths of 10 km s^{-1}. The range of $n(\mathrm{H_2})$ covers $\sim$0.01 to $\sim$100 times the critical density of the ^{13}CO $J = 3 \rightarrow 2$ line. The hatched area corresponds to observed positions in NGC 253 and M83.

the emitting gas based on the low $^{13}R_{32}$ values (typically less than 0.1 outside the inner 20″) in the sample galaxies. The LVG results confirm the low molecular gas densities inferred in § 3.2 from LTE considerations. Three quantities affect the excitation of the ^{13}CO lines: the kinetic temperature, T_K, density of colliding molecules, $n(\mathrm{H_2})$, and the ^{13}CO column density per velocity interval, $N(^{13}\mathrm{CO})/\Delta V$. Figure 7 illustrates contours of constant $^{13}R_{32}$ as a function of $N(^{13}\mathrm{CO})/\Delta V$ and $n(\mathrm{H_2})$ for T_K fixed at 10 K. We chose 10 K to be the representative T_K for Figure 7 because this is the lowest likely temperature for the molecular gas (see Table 6) and because a low T_K permits higher densities to satisfy the observational constraints. The range of $N(^{13}\mathrm{CO})/\Delta V$ corresponds to a range in $N(\mathrm{H_2})$ of 10^{20}–10^{24} cm^{-2} (i.e., $A_v \simeq 0.1$–1000 mag) assuming a ^{12}CO/^{13}CO abundance ratio of 30 and assuming $\Delta V_{\mathrm{cloud}} = 10$ km s^{-1}. Figure 7 suggests that, even for molecular gas as cold as 10 K, the density must be less than 10^3 cm^{-3} outside the inner 20″ diameter (but still inside the central 60″ diameter). Even allowing a factor of 3 uncertainty in the upper limits on $^{13}R_{32}$, $n(\mathrm{H_2})$ must be less than 3×10^4 cm^{-3}.

The observed $^{13}R_{32}$ upper limit places an upper limit on the amount of high-density [i.e., in LTE or $n(\mathrm{H_2}) \gtrsim 5 \times 10^4$ cm^{-3}] gas present in the central $\sim$1 kpc (60″) diameters, excluding the central few hundred parsecs (i.e., 20″), of the sample galaxies. High-density gas with $T_K \geq 10$ K can contribute no more than 20% to the molecular gas mass if the ^{13}CO lines are optically thin. Allowing $\tau(^{13}\mathrm{CO}\ J = 2 \rightarrow 1)$ to be as high as 3 still limits the dense gas to $\lesssim$50% of the mass of molecular gas, if a model which includes some dense gas is to be consistent with the ^{13}CO and ^{12}CO data. It is possible, however, to account for both the observed $^{13}R_{32}$ and $^{12}R_{32}$ ratios with two dense (LTE) components and no tenuous gas. A cold ($T_K \leq 5$ K) component would have to dominate the ^{13}CO line emission and a warm ($T_K \geq 20$ K) component would have to dominate the ^{12}CO line emission. The warm component must be optically thin in the ^{12}CO lines [e.g., $\tau(^{12}\mathrm{CO}\ J = 2 \rightarrow 1) \lesssim 0.3$) so that its ^{13}CO emission would not dominate that of the cold component. Obtaining an estimate of $^{13}R_{21}$ from ^{13}CO $J = 1 \rightarrow 0$ observations (with $\sim$20″ resolution) could rule out cold gas dominating the ^{13}CO emission if $^{13}R_{21} \gtrsim 1$—as observed in M82 (where $^{13}R_{21} = 2$; see Tilanus et al. 1991).

There is additional evidence for low-density molecular gas in NGC 253 and M82. The value of $^{12}R_{32}$ observed toward the ends of the $\sim$40″ × 10″ ($\sim$480 pc × 120 pc) gas bar in NGC 253 requires $n(\mathrm{H_2}) \lesssim 10^4$ cm^{-3} if $T_K \geq 10$ K (Wall et al. 1991). In M82, over a 40″ diameter, Tilanus et al. (1990) found $n(\mathrm{H_2}) \lesssim 10^4$ cm^{-3} from both ^{12}CO and ^{13}CO lines.

The excitation conditions prevalent in the inner 60″ of the galaxies in our sample are similar to those in low column density "diffuse" clouds and at giant molecular cloud boundaries in our Galaxy. Van Dishoeck et al. (1991) derive $n(\mathrm{H_2}) \sim 10^3$ to 10^4 cm^{-3} for translucent and high-latitude clouds from ^{12}CO $J = 3 \rightarrow 2$ and ^{12}CO $J = 2 \rightarrow 1$ observations. Falgarone, Phillips, & Walker (1991), observing edge regions in the Taurus molecular complex, have made some of the only observations of $J = 3 \rightarrow 2$ and $J = 2 \rightarrow 1$ ^{12}CO and ^{13}CO lines away from the centers of molecular clouds. Reanalysis of their data shows that they are not inconsistent with densities of less than 10^4 cm^{-3}. Figure 7 of Falgarone et al. is a contour map of $^{12}R_{32}$ and $\tau(^{12}\mathrm{CO}\ J = 2 \rightarrow 1)$ values as functions of LVG model densities and column densities per velocity interval, which suggests that only densities $\gtrsim 10^4$ cm^{-3} are consistent with the uncertainty in $\tau(^{12}\mathrm{CO}\ J = 2 \rightarrow 1)$. We have compared their observed ^{13}CO $J = 2 \rightarrow 1$/^{12}CO $J = 2 \rightarrow 1$ intensity ratio [*different from* $\tau(^{13}\mathrm{CO}\ J = 2 \rightarrow 1)$ *in the non–LTE case* and, hence, not directly relatable to $\tau(^{12}\mathrm{CO}\ J = 2 \rightarrow 1)$] to LVG models and find that densities down to 10^3 cm^{-3} are consistent with the observations. In addition, Falgarone et al. observe an upper limit to the ^{13}CO $J = 3 \rightarrow 2$ line, which would give $\tau(^{13}\mathrm{CO}\ J = 3 \rightarrow 2)/\tau(^{13}\mathrm{CO}\ J = 2 \rightarrow 1) < 0.17$ in LTE. This ratio requires $T_K = 5$ K in LTE which, after applying the Rayleigh-Jeans correction, corresponds to a ^{12}CO $J = 2 \rightarrow 1$ line radiation temperature of less than 0.5 of what they observe. Hence, their ^{13}CO $J = 3 \rightarrow 2$ upper limit also provides good evidence for molecular gas densities lower than $\sim 5 \times 10^4$ cm^{-3}.

There is also evidence that the bulk of ^{12}CO-emitting gas in the inner Galaxy is at low densities [$n(\mathrm{H_2}) \sim 10^3$ cm^{-3}]. The Far-InfraRed Absolute Spectrophotometer (FIRAS) experiment aboard the *COsmic Background Explorer* (*COBE*) spacecraft detected the $J = 2 \rightarrow 1$, $3 \rightarrow 2$, $4 \rightarrow 3$, and $5 \rightarrow 4$ lines of ^{12}CO, whose intensities, averaged over the entire Galaxy (although dominated by emission from inside the solar circle), have been computed (Wright et al. 1991). The $^{12}R_{32}$ ratio is 0.4 (as opposed to the flux ratio of 1.4), which is similar to that observed in IC 342 (Wall & Jaffe 1990) and implies $n(\mathrm{H_2}) \lesssim 5 \times 10^4$ cm^{-3}. The alternative LTE scenario requires $T_K = 4$ K, resulting in a ^{12}CO $J = 1 \rightarrow 0$ line weaker than observed for most of the first Galactic quadrant (Sanders, Scoville, & Solomon 1985). LVG modeling of the four lines observed by FIRAS suggests $n(\mathrm{H_2}) \sim 10^3$ cm^{-3} for the bulk of the ^{12}CO-emitting gas.

4.1.3. *A Two-Component Scenario*

The observations presented in §§ 3, 4.1.1, and 4.1.2 demonstrate that we cannot use a simple model to explain the ISM in

the inner 500–1600 pc of the galaxies in our sample. The strong gradient in CO line ratios from the central beam to the immediately adjacent regions in most galaxies (see Table 6) and the large variations from galaxy to galaxy, imply that no single temperature-density component can match all of the molecular line data, especially when observations of transitions from molecules with large dipole moments, like CS, HCO^+, and HCN, are included. Wall & Jaffe (1990) used the available moecular line data for IC 342 to argue for a simple but plausible two-component model for the molecular gas in the inner region of that galaxy: a high-density component [$n(H_2) \gtrsim 10^4$ cm^{-3}] dominating the ^{13}CO emission and a low-density component [$n(H_2) \lesssim 10^3$ cm^{-3}] dominating the ^{12}CO emission. In this section, we summarize the Wall & Jaffe model for IC 342 and see if some version of this model applies to the inner ~ 1 kpc regions of the other galaxies in our sample (i.e., those listed in Table 6).

The first component in the Wall & Jaffe model for IC 342 consists of warm ($T_K \sim 50$ K), dense [$n(H_2) \gtrsim 10^4$ cm^{-3}] cores with high column densities [$N(H_2) \sim 10^{24}$ cm^{-2}] and a modest area filling factor ($\eta_{ff} = 6 \times 10^{-3}$ in a 24″ beam). The dense cores may well be concentrated in the narrow filaments seen in the ^{12}CO and ^{13}CO $J = 1 \rightarrow 0$ interferometer maps of the inner arcminute of the galaxy (Ishizuki et al. 1990; Turner & Hurt 1992). The dense gas can account not only for the bulk of the emission in the ^{13}CO lines, but also for the low-J line emission from molecules with high-dipole moments. The close association of ^{13}CO and high-dipole moment molecules in IC 342 is supported by the observations of Nguyen-Q-Rieu et al. (1992) who find the flux in the HCN $J = 1 \rightarrow 0$ line to be identical to that in the ^{13}CO $J = 1 \rightarrow 0$ line in similar-sized beam. Israel (1992) obtains a similar result for his sample of six galaxies in which the HCN $J = 1 \rightarrow 0/^{13}CO$ $J = 1 \rightarrow 0$ and HCO^+ $J = 1 \rightarrow 0/^{13}CO$ $J = 1 \rightarrow 0$ intensity ratios vary by less than a factor of 2 about their mean values.

The second component of molecular gas is necessary in IC 342 because a single component with optically thick ^{13}CO lines has ^{12}CO lines that are even more opaque and, hence, more excited by radiative trapping, resulting in $^{12}R_{32} \geq {}^{13}R_{32}$. However, $^{12}R_{32} < {}^{13}R_{32}$ was observed, requiring a separate component responsible for the ^{12}CO emission. (Note that merely having *both* the ^{13}CO *and* ^{12}CO lines optically thick whereas the ^{12}CO lines are 5–10 times stronger is *not* sufficient reason to require a second molecular gas component: radiative trapping effects are much stronger in ^{12}CO lines, allowing them to thermalize, even at densities low enough for subthermal effects in the ^{13}CO lines.) Wall & Jaffe attribute the ^{12}CO emission to a combination of PDRs on the surface of the ^{13}CO-emitting dense cores and an ensemble of low-density, low-column density "tiny little clouds" (Knapp & Bowers 1988). Alternatively, the low-density, low-column density gas could either originate from the tenuous [$n(H_2) \sim 10^3$ cm^{-3}] envelopes separated from dense cloud cores by tidal stresses (Stark et al. 1989) or from the "spray" resulting when molecular gas traveling in one family of orbits in a barred potential collides with molecular gas traveling in another family of orbits (Binney et al. 1991). If this low-density gas has high area filling factor and low column density, it should contribute significantly to the $J = 1 \rightarrow 0$ and $2 \rightarrow 1$ ^{12}CO lines without contributing appreciably to either the higher J lines or to isotopic CO lines.

Two molecular gas components are also inferred in the other sample galaxies: a warm ($T_K \gtrsim 50$–100 K), dense [$n(H_2) \gtrsim 10^4$ cm^{-3}] component and a low-density [$n(H_2) \lesssim 10^3$–10^4 cm^{-3}] component. In the sample galaxies, the components manifest themselves as high-$^{13}R_{32}$ gas (e.g., $\simeq 2$ in the central ~ 240 pc diameter of NGC 253) and low-$^{13}R_{32}$ gas (e.g., $\lesssim 0.2$ just outside this central region in NGC 253 and in the central ~ 1 kpc diameter of M83), except in IC 342, where $^{13}R_{32} \simeq 1$ in the high-density component and $^{13}R_{32}$ is irrelevant in the low-density component (because the ^{13}CO lines are so much weaker than the ^{12}CO lines in this component). The difference between the observational properties of IC 342's molecular gas components and those of the other sample galaxies can be attributed to column density. For example, decreasing the column density of IC 342's high-density component will reduce the opacity in the ^{13}CO lines allowing $^{13}R_{32}$ to rise above unity (since this gas is warm). Conversely, increasing the column density of IC 342's low-density component strengthens the ^{13}CO lines relative to the ^{12}CO lines, but retains a small $^{13}R_{32}$ (since this gas is low density). Hence, by merely adjusting the column densities and relative amounts of these two components the observed $^{13}R_{32}$ and $^{12}R_{32}$ are reproduced in all sample galaxies.

4.1.4. *Gas Dynamics and the Warm, Dense Component*

In this section, we assess whether the warm, dense component discussed in the previous section can be totally accounted for by dynamics (e.g., tides or turbulence) rather than by star formation. The warm, dense molecular gas component is found preferentially in the central few hundred parsecs of the sample galaxies. This is not to say that warm, dense molecular gas does not exist outside the central regions—indeed, $^{13}R_{32}$ has not yet been completely mapped in the central kiloparsec of the sample galaxies—but our limited data suggest a preference of the warm, dense molecular gas for the central 170–530 pc regions [$^{12}R_{32}(20'') > {}^{12}R_{32}(60'')$, as shown in Table 6, and $^{13}R_{32}$ is centrally peaked in NGC 253 and M83]. It is in these central few hundred parsecs that, as in our Galaxy (see Güsten 1989), tidal forces and turbulence are at their strongest. Accordingly, it is reasonable to assume some connection between the warm, dense molecular gas and the unique dynamics of the central regions.

The high densities [$n(H_2) \gtrsim 10^4$ cm^{-3}] defining the warm, dense molecular gas component are also present in the center of our Galaxy, where the molecular gas in the central few hundred parsecs is an order of magnitude denser than the gas in the disk (Bally et al. 1988). The high gas densities in the Galactic center are explained by tidal stripping of the tenuous envelopes of the molecular clouds, leaving only cloud interiors dense enough [i.e., $n(H_2) \gtrsim 10^4$ cm^{-3}, see Güsten 1989] to survive tidal stresses. While tidal forces may partly account for the tendency of dense gas to inhabit the central regions of the sample galaxies, they do not explain differences between the centers of the sample galaxies: e.g., why dense gas is predominant in the center of NGC 253, but is scarce in the center of M83 (but not wholly absent, as indicated by observations of high-dipole moment molecules; Mauersberger & Henkel 1989; Nguyen-Q-Rieu et al. 1989; Israel 1992). The rotational velocity gradient averaged over the central 20″ (360 pc) of M83 is 40% higher than that in NGC 253 (Canzian et al. 1988; Nanda et al. 1990), implying a minimum density 2 times *higher* than that in NGC 253 [using $n(H_2)_{min} \propto (V_{rot}/R)^2$; see Stark et al. 1989]. Also, within the central arcminute of NGC 253 and of M83, the steepely rising portion of the rotation curve (see Canzian et al. 1988 and Handa et al. 1990) occurs in the same

size region (i.e., within $\sim$120–150 pc, although the Canzian et al. data do not extend much beyond this). Therefore, it is likely that tidal effects alone do not account for the preference of the dense gas for the central few hundred parsecs of these galaxies. Indeed, the rotational gradient in the central 200 pc diameter of NGC 253 (0.6 km s^{-1}) is $\sim\frac{1}{3}$ that in the central 200 pc diameter of our Galaxy (see Canzian et al. 1988 and Oort 1977 and references therein), implying minimum densities of only $n(H_2) \sim 10^3$ cm^{-3}—one or two orders of magnitude lower than the inferred lower limit of Wall et al. (1991).

Although turbulent heating may explain the high kinetic temperatures inferred in the center of our Galaxy (i.e., $T_K \gtrsim 70$ K; see Güsten 1989), the arguments presented above and the high far-UV energy densities inferred from [C II] 158 μm observations for some of these galaxies (Crawford et al. 1985; Wolfire, Hollenbach, & Tielens 1989; Stacey et al. 1991), suggest that the warm, dense component is associated with star formation and that dynamical effects are not entirely responsible for this warm, dense gas. The bias of star formation toward high-density regions is consistent with near-IR and CS $J = 2 \rightarrow 1$ surveys of Orion B, which show star clusters only in or near the dense cores of the molecular cloud (Lada 1992).

4.2. *Gas and Stellar Masses*

The lower limits to the mass of molecular gas in the central 1′ (500–1600 pc) diameter regions of the sample galaxies [$M(H_2) \gtrsim 3$ to 7×10^7 $M_\odot$; see Table 7] are comparable to the mass of molecular gas in the central 1 kpc diameter of our Galaxy ($\sim 10^8$ $M_\odot$; Bally et al. 1988). The mass of the ISM relative to the stellar mass (approximated by M_{dyn}) in the sample galaxies is $\gtrsim$3%–10%, whereas in the central 1 kpc diameter of our Galaxy it is only 1%–2% (using a stellar mass of 5–10 $\times 10^9$ $M_\odot$; Oort 1977). Hence, the sample galaxies are enriched in gas mass relative to stellar mass, compared to a roughly equivalent region in our Galaxy, by factors of $\gtrsim$2–10. Our $M(H_2)$ values for the sample may be underestimates for the following reasons:

1. Some of the ^{13}CO lines are optically thick, as found in IC 342 [e.g., $\tau(^{13}\mathrm{CO}\ J = 2 \rightarrow 1) \simeq$ 1–3; Wall & Jaffe 1990] and in NGC 253 [i.e., $\tau(^{13}\mathrm{CO}\ J = 1 \rightarrow 0) \simeq$ 1–5]. Our mass estimates would then be low by factors $\lesssim$5.
2. The densities may be low enough [i.e., $n(H_2) \lesssim 10^3$ cm^{-3}] that non-LTE effects would underestimate the column densities derived from the ^{13}CO integrated line strengths in the LTE approximation.
3. The kinetic temperatures adopted in deriving the column densities from the ^{13}CO and C^{18}O integrated line strengths is uncertain, because the kinetic temperatures assumed from $^{13}R_{32}$ or $^{12}R_{32}$ are only lower limits. For instance, if we had chosen $T_K = 50$ K in IC 342, as Wall & Jaffe (1990) did for the central 20″, instead of $T_K = 20$ K from $^{13}R_{32} = 1.0$, we would derive a mass 3 times higher than that in Table 7 (since for fixed τ, the derived column density increases with increasing T_K).
4. The $N(H_2)$-to-$\int T_{MB}(^{12}\mathrm{CO})dV$ conversion ratios computed from the ^{13}CO observations of the central 20″ of the sample galaxies may be smaller than appropriate over the inner 60″ diameter. This would parallel the situation in our Galaxy where the $N(H_2)$-to-$\int T_{MB}(^{12}\mathrm{CO}\ J = 1 \rightarrow 0)dV$ conversion factor for the central 400 pc is as much as 10 times smaller than in the first Galactic quadrant (Blitz et al. 1985). It is interesting to note that the conversion factors derived for the central 20″ diameters, using ^{13}CO-derived column densities, are in the range 1–4 $\times 10^{19}$ cm^{-2} (K km s^{-1})$^{-1}$ — $\sim$10 times smaller than the canonical conversion factor.

Making allowances for the problems above could give molecular gas mass estimates closer to those of previous work (e.g., Scoville et al. 1985; Young & Scoville 1984), which used the canonical $N(H_2)$-to-$\int T_{MB}(^{12}\mathrm{CO}\ J = 1 \rightarrow 0)dV$ conversion factor. On the other hand, since the central regions of these galaxies may be enriched in metals, it is quite possible that the CO abundance adopted [i.e., $X(^{12}\mathrm{CO}) = 10^{-4}$] is too low and the masses listed in Table 7 are overestimates. For example, the O/H abundance ratio in the central $\sim$1′ of M83 is $\sim$2–5 times the solar value (Dufour et al. 1980), suggesting that the CO/H_2 abundance ratio *could* be higher than the value (i.e., 10^{-4}) assumed in this paper.

4.3. *Total* CO *Luminosity*

The total luminosity emitted by all CO rotational lines, $L_{tot}(CO)$, in our sample galaxies can be estimated from the LVG models and the luminosity of the $^{12}\mathrm{CO}\ J = 3 \rightarrow 2$ lines, L_{32}. We find that $L_{32}/L_{tot}(CO) = 0.1$ to within a factor of 5 (i.e., 0.02–0.4) for $T_K = 10$–50 K, $n(H_2) = 10^2$–10^5 cm^{-3}, and for $N(CO)/\Delta V = 10^{17}$–10^{18} cm^{-2} (km s^{-1})$^{-1}$ [corresponding to $N(H_2) \simeq 10^{22}$–10^{23} cm^{-2}, or $A_v \simeq 10$–100 mag, for clouds with $\Delta V = 10$ km s^{-1}]. The $^{12}\mathrm{CO}\ J = 3 \rightarrow 2$ luminosity is a better estimator of $L_{tot}(CO)$ than the $^{12}\mathrm{CO}\ J = 1 \rightarrow 0$ luminosity, L_{10}, because L_{32} is $\sim$10% of $L_{tot}(CO)$ whereas L_{10} is only $\sim$0.4% of $L_{tot}(CO)$. For our Galaxy, $L_{tot}(CO)$ was computed by adding the luminosities of the individual ^{12}CO lines detected by FIRAS (Wright et al. 1991) and applying a 20%–30% correction for those ^{12}CO lines not observed, as suggested by the LVG modeling. $L_{tot}(CO)$ varies from $\sim 10^5$ to $\sim 10^6$ $L_\odot$ (see Table 8), which corresponds to $L_{tot}(CO)/L_{FIR} \sim 10^{-4}$ to 10^{-3}, where L_{FIR} is the far-IR luminosity. The modeling suggests that 90% of $L_{tot}(CO)$ is radiated in the first four to eight rotational lines of ^{12}CO. In comparison, the luminosity in the single [C II] 158 μm line (which arises in dense atomic gas closely associated with molecular gas) is 10^{-3} to 10^{-2} of L_{FIR} (Stacey et al. 1991; Wright et al. 1991).

4.4. *Photodissociation Regions and Molecular Gas Heating*

The far-UV field is important in heating photodissociation regions (PDRs) which, in turn, could be responsible for much of the CO emission (see Wolfire et al. 1989). The mass of molecular gas in each galaxy, $M(H_2)$, estimated from the ^{13}CO lines, along with the far-IR luminosity, L_{FIR}, can be used to estimate the average far-UV field. Assume the molecular gas consists of identical spherical clumps of mass m_c and uniform density $n(H_2)$. The surface area, S, of all the clumps is then given by

$$S = 36.0 M(H_2) m_c^{-1/3} [n(H_2)]^{-2/3} , \quad (1)$$

where S is in pc^2, $M(H_2)$ and m_c are in $M_\odot$, and $n(H_2)$ is in cm^{-3}. The weak dependence of S on m_c is to the $-\frac{1}{3}$ power because the surface area of each clump goes like $m_c^{2/3}$, but the number of clumps goes like m_c^{-1}. If essentially all the far-UV radiation is absorbed by dust in molecular clouds, then it will be reprocessed into IR and the far-UV energy intensity, G_0, is given by L_{FIR}/S, so that

$$G_0 = 7.11 \times 10^{-3} L_{FIR} [M(H_2)]^{-1} m_c^{1/3} [n(H_2)]^{2/3} , \quad (2)$$

where L_{FIR} is in $L_\odot$ and G_0 in Habing units ($G_0 = 1$ corresponds to the average interstellar radiation field in our

TABLE 8

TOTAL CO LUMINOSITY AND FAR-UV ENERGY DENSITY

GALAXY	$L_{tot}(CO)$ ($L_\odot$)	$L_{[C\ II]}$ ($L_\odot$)	L_{FIR} ($L_\odot$)	$L_{tot}(CO)/L_{FIR}$	LOG G_0	
					L_{IR}/S	$I_{[C\ II]}$
NGC 253	3×10^6	...	1.5×10^{10} [a]	2×10^{-4}	3.6	...
IC 342	2×10^5	2.6×10^6 [b]	6×10^8 [c]	3×10^{-4}	3.0	3.1 [d]
M83	1×10^6	1.7×10^7 [b]	4×10^9 [a]	3×10^{-4}	2.7	3.1 [d]
NGC 6946	3×10^6	6.3×10^6 [b]	5×10^9 [a]	6×10^{-4}	2.9	2.8 [d]
Maffei 2	4×10^6	1.3×10^7 [b]	6×10^9 [e]	7×10^{-4}	2.9	3.1 [b]
M82	3×10^6	4.9×10^7 [b]	3×10^{10} [a]	1×10^{-4}	3.5	3.4 [d]
Milky Way [f]	4×10^5 [g]	5.0×10^7 [g]	2×10^{10} [g]	2×10^{-5}	1.8 [h]	...

[a] Telesco & Harper 1980 scaled to our distance.
[b] Stacey et al. 1991 scaled to our distances for $L_{[C\ II]}$.
[c] Becklin et al. 1980 scaled to $D = 1.8$ Mpc.
[d] Wolfire et al. 1989.
[e] Computed from *IRAS* Point Source Catalog 1985.
[f] Predominantly emission from inside solar circle, as opposed to central ~ 1 kpc diameter (as in other sampled galaxies).
[g] Wright et al. 1991 increased by 25%, as approximate correction for undetected lines.
[h] Using $M(H_2)$ from Sanders et al. 1985.

Galaxy). Note that the expression for G_0 above is independent of the adopted distance to the galaxy. This particular form of equation (2) is useful because G_0 depends only weakly on clump parameters [i.e., $n(H_2)$ and particularly m_c]. We choose m_c to be a tiny fraction of the mass of a giant molecular cloud, since giant molecular clouds consist of many clumps much smaller that the cloud itself (e.g., M17SW; see Stutzki & Güsten 1990). We adopt $m_c = 20\ M_\odot$ and $n(H_2) = 10^4\ cm^{-3}$, giving

$$G_0 = 8.96 L_{FIR}[M(H_2)]^{-1}\ . \quad (3)$$

The G_0 derived is an upper limit (unless a substantial fraction of the far-UV escapes) since our masses are lower limits. Our upper limits to G_0 are shown in Table 8, along with estimates of G_0 from Wolfire et al. (1989), who used the [C II] 158 μm, $^{12}CO\ J = 1 \rightarrow 0$ line intensities and the far-IR intensity. Both the Wolfire et al. G_0 estimates and our G_0 estimates apply to the central $\sim 60''$ diameter of each galaxy. Our upper limits to G_0 are consistent with the Wolfire et al. estimates to within a factor of 3. Our adopted clump density and mass results in agreement between the two methods, supporting the idea that PDRs play an important role in the emission of CO lines in infrared-bright galaxies (Crawford et al. 1985; Stacey et al. 1991).

4.5. *Star Formation Activity in the Central 20″*

Column densities from the ^{13}CO lines, along with Hα data from the literature, can be used to compare the star formation rate per unit mass, or star formation "activity," in the inner few hundred parsecs of the sample galaxies with that in the outer disks of spiral galaxies. Kennicutt (1989) used the surface brightness of the Hα line, $\Sigma(H\alpha)$, uncorrected for extinction effects, as a measure of massive star formation rate. The $\Sigma(H\alpha)$ was compared to the surface mass density of the interstellar medium, Σ_H [$= \Sigma(H_2) + \Sigma(H\ I)$], derived from $^{12}CO\ J = 1 \rightarrow 0$ and 21 cm H I observations of a sample of spiral galaxies. Kennicutt found that the massive star formation activity is roughly constant [i.e., $\Sigma(H\alpha) = (\Sigma_H)^n$ with an index $n \simeq 1.3$], provided that Σ_H surpasses some critical value [here $\Sigma_H(\text{critical}) \sim 3\ M_\odot\ pc^{-2}$]. The Kennicutt data, however, apply only to the outer disks of a sample of spiral galaxies. Our ^{13}CO data, along with published Hα data (see Fig. 8 caption), allow us to test the Kennicutt relationship for our small sample of galactic nuclei.

Figure 8 shows Kennicutt's $\Sigma(H\alpha)$ versus Σ_H data and the extension provided by our data. The stars in the upper right corner represent values for the inner 20″ of galaxies in our sample. The horizontal position of each open star shows the value of Σ_H for each galaxy estimated from the $^{13}CO\ J = 2 \rightarrow 1$ integrated intensity assuming this line is optically thin. The horizontal error bar gives the maximum likely range of Σ_H values based on this measurement; the upper limit on Σ_H is close to the Σ_H value derived from the standard $N(H_2)/\int T_{MB}(^{12}CO\ J = 1 \rightarrow 0)$ conversion factor. The extreme conditions in the nuclei of starburst galaxies may invalidate the canonical $N(H_2)/\int T_{MB}(^{12}CO\ J = 1 \rightarrow 0)$ relationship (e.g., see Maloney & Black 1988). The vertical position of each open star shows the value of $\Sigma(H\alpha)$ assuming *zero* extinction. The vertical error bars represent possible corrections due to extinction. Although Kennicutt did not apply extinction corrections to his Hα data, the extinction at Hα in the central $\sim 20''$ is high enough (i.e., $A_v \sim 5$–50 mag; Rieke et al. 1980; Lester et al. 1990; Turner, Ho, & Beck 1987a; Lebofsky & Rieke 1979; de Gioia-Eastwood et al. 1984) that correcting for the central extinction is necessary for a meaningful comparison with the relatively unextincted Hα emission from the outer disks. Since the extinction estimates for the center of a given galaxy can vary greatly (e.g., $A_v \simeq 5$–25 mag for M82; see Lester et al. 1990; Rieke et al. 1980) we adopt $A_v = 10$ mag for the extinction, a representative value that lies in the range of values normally encountered. Assuming the dust to be evenly distributed among the stars, instead of lying in a foreground screen, the upward correction is a factor of 10 in $\Sigma(H\alpha)$ (e.g., see Thronson et al. 1990) or more than 10 if the stars are more centrally condensed than the dust. Each vertical error bar illustrates this factor of 10 uncertainty in $\Sigma(H\alpha)$, where the arrow represents a possible further upward correction if the stars are more centrally positioned than the dust. The dotted line extending to the right edge of Figure 8 represents points of constant star formation activity, which has been fitted to the data of Kennicutt (1989) for $\log \Sigma_H \geq 0.9$. The dashed lines represent the maximum and minimum likely slopes of lines

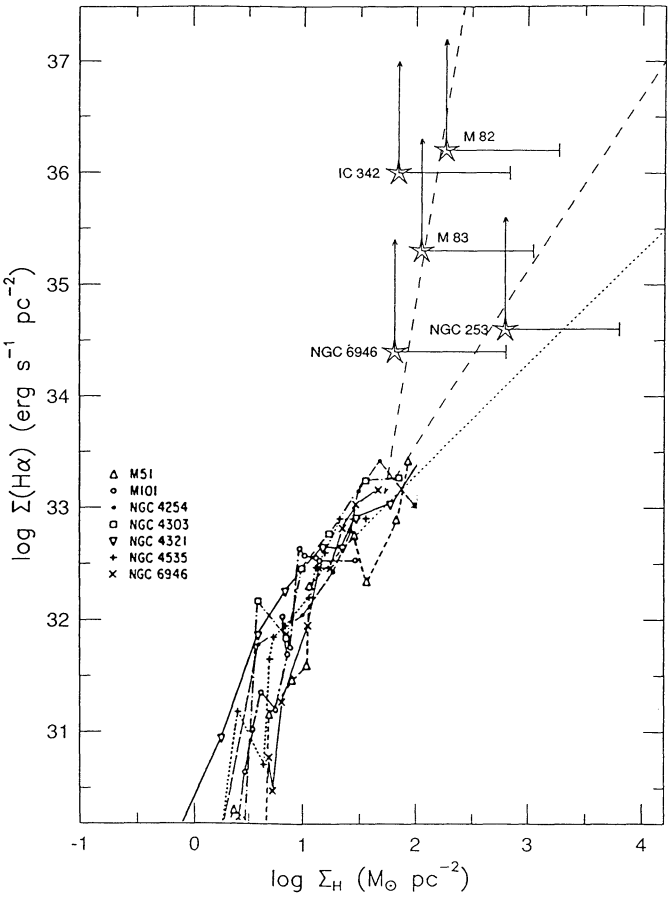

FIG. 8.—The Hα surface brightness, uncorrected for extinction effects, is plotted against gas surface density in a small sample of galaxies. The lower left corner of the plot contains a figure from the work of Kennicutt (1989, reprinted with the author's permission), which illustrates the Hα surface brightness vs. gas surface density averaged over concentric annuli outside the central 4 kpc diameter for each galaxy in Kennicutt's original figure. The stars in the upper right corner of the plot show the Hα surface brightness vs. gas surface density for the central 20″ (170–530 pc) diameters of the galaxies in our sample. The error bars represent possible upward corrections to Σ_H and Σ(Hα) (see § 4.5). The Hα surface brightnesses were taken from the literature (i.e., Keel 1984; McCarthy et al. 1987; de Vaucouleurs et al. 1983, de Gioia-Eastwood et al. 1984) and the gas surface densities were derived from ^{13}CO integrated line strengths (^{13}CO $J = 2 \rightarrow 1$ data for M82 from Loiseau et al. 1990). The Hα surface brightness for IC 342 was multiplied by 10 to account for a recent revision to the Galactic extinction toward IC 342 (McCall 1989). The dashed lines depict the maximum and minimum slopes (i.e., 5.6 and 1.4) representing our sample and determined by *fixing* the lines to the "end" of the Kennicutt sample and *fitting* to the points at the ends of our vertical and horizontal error bars, respectively. The best fit to our data (not shown) has a slope of 2.8. The dotted line that extends to the right edge of the plot represents a line of constant star formation rate per unit mass, fitted to the Kennicutt data for $\log \Sigma_H \geq 0.9$.

fixed to the "end" of the Kennicutt data and *fitted* to our sample. The maximum and minimum slopes (i.e., 5.6 and 1.4) were determined from fitting to the points at the ends of the vertical and horizontal error bars, respectively. The minimum slope of 1.4 is only marginally larger than the Kennicutt slope of 1.3, but this represents the extreme case of using the standard conversion factor for Σ_H. The direct fit to the open stars data, including the fixed point at the end of the Kennicutt sample, has a slope of 2.8. Figure 8 demonstrates, for our small sample, that the star formation activity [as indicated by Σ(Hα) vs. Σ_H] is higher in the central few hundred parsecs than that found in the outer disks (outside the central ~4 kpc diameter regions) of spiral galaxies. Alternatively, the higher Σ(Hα) versus Σ_H slope could be due to a higher low mass cutoff of the IMF in the central regions than that for the outer disks.

The heightened star formation activity suggested in Figure 8 is consistent with the results of Krügel et al. (1988), who found that the star formation rate (represented by far-IR luminosity) per unit mass (from millimeter continuum fluxes) is an order of magnitude higher for a group of "active" galaxies, including NGC 253 and M82, than for other "nonactive" galaxies. Comparison of the Krügel et al. study with our Figure 8 is not strictly valid because Krügel et al. compare equivalent regions of different galaxies, whereas we compare the central regions of *our sample* galaxies with the outer star-forming disks of *other* galaxies. Nevetheless, both our study and that of Krügel et al. show that the star formation activity can be enhanced in galactic nuclei beyond what one expects from a simple power-law extrapolation of emission from galactic disks.

5. CONCLUSIONS

The picture that emerges for the molecular gas in our sample of infrared-bright galaxies is that of warm ($T_K \gtrsim 20$ K), low-density [$n(H_2) \lesssim 10^4$ cm^{-3}] molecular clouds with column densities possibly exceeding 10^{23} cm^{-2} ($A_v \gtrsim 100$ mag). The molecular gas accounts for at least 3%–10% of the mass in the central ~1 kpc diameters—factors of ~2–10 higher than that in the equivalent region in our Galaxy. An additional warmer ($T_K \gtrsim 50$ K), high-density [$n(H_2) \gtrsim 10^4$–10^5 cm^{-3}] component also exists in the central few hundred parsecs, as most clearly exemplified in NGC 253. We associate the high-density component with the warm, dense molecular cores observed in Galactic star forming regions (e.g., Orion B; Lada 1992) and argue that dynamical effects cannot entirely account the existence of this warm, dense molecular gas. The molecular gas in the inner few hundred parsecs demonstrates enhanced star formation activity with respect to that observed in the outer regions of the star-forming disks of spiral galaxies.

The temperatures and densities of the two molecular cloud components described above can be crudely represented by different *parts* of the Orion molecular complex. The Orion B molecular cloud has only few percent by mass of the dense [$n(H_2) \gtrsim 10^5$ cm^{-3}] CS $J = 2 \rightarrow 1$ emitting gas (see Lada 1992; Maddalena 1986) and the radiation temperature of the ^{12}CO $J = 1 \rightarrow 0$ line suggests kinetic temperatures of 5–10 K over most of the cloud's area (Maddalena 1986). In contrast, the hot core of the Orion A molecular cloud has very warm ($T_K \gtrsim 150$ K) and dense [$n(H_2) \gtrsim 10^7$ cm^{-3}] molecular gas (see Genzel & Stutzki 1989 and references therein). The molecular line emission from the central kiloparsec of the sample galaxies may be dominated by molecular clouds similar to Orion B, while that of the central few hundred parsecs has a contribution from clouds similar to the Orion A hot core region.

Further work is required to confirm the results of this paper. More extensive mapping of the $J = 3 \rightarrow 2$ and $J = 2 \rightarrow 1$ lines of ^{13}CO is needed, both in the current galaxy sample and for other external galaxies. Observations of the ^{13}CO $J = 1 \rightarrow 0$ and C^{18}O $J = 1 \rightarrow 0$ and C^{18}O $J = 2 \rightarrow 1$ lines would help to further constrain excitation models.

We thank N. Evans, Y. Wang, and R. Plume for helping with the observations. Special thanks to the staff of the CSO, who made the ^{13}CO $J = 3 \rightarrow 2$ observations possible. The CSO is

operated by the California Intitute of Technology under funding from the National Science Foundation, Grant No. AST 88-15132. This work was supported in part by NSF Grant No. AST 88-15801 to the University of Texas at Austin and by a grant from the W. M. Keck Foundation. Support was also provided by a Texas Advanced Research Project Grant. This work was completed while W. F. W. held a National Research Center-NASA/GSFC Research Associateship. D. J. acknowledges support from a David and Lucile Packard Foundation Fellowship.

REFERENCES

Bally, J., Stark, A. A., Wilson, R. W., & Henkel, C. 1988, ApJ, 324, 223
Becklin, E. E., Gatley, I., Matthews, K., Neugebauer, G., Sellgren, K., Werner, M. W., & Wynn-Williams, C. G. 1980, ApJS, 57, 535
Binney, J., Gerhard, O. E., Stark, A. A., Bally, J., & Uchida, K. I. 1991, MNRAS, 252, 210
Blitz, L., Bloemen, J. G. M., Hermsen, W., & Bania, T. M. 1985, A&A, 143, 267
Canzian, B., Mundy, L. G., & Scoville, N. Z. 1988, ApJ, 333, 157
Carignan, C., Charbonneau, P., Boulanger, F., & Viallefond, F. 1990, A&A, 234, 43
Casoli, F., Clausset, F., Viallefond, F., Combes, F., & Boulanger, F. 1990, A&A, 233, 357
Combes, F., Gottesman, S. T., & Weliachew, L. 1977, A&A, 59, 181
Crawford, M. K., Genzel, R., Townes, C. H., & Watson, D. M. 1985, ApJ, 291, 755
Crutcher, R. M., Rogstad, D. H., & Chu, K. 1978, ApJ, 225, 784
de Gioia-Eastwood, K., Grasdalen, G. L., Strom, S. E., & Strom, K. M. 1984, ApJ, 278, 564
de Jong, T., Chu, S. I., & Dalgarno, A. 1975, ApJ, 199, 69
de Vaucouleurs, G. 1979, AJ, 84, 1270
de Vaucouleurs, G., Pence, W. D., & Davoust, E. 1983, ApJS, 53, 17
Dickman, R. L. 1975, ApJ, 202, 50
Dufour, R. J., Talbot, R. J., Jensen, E. B., & Shields, G. A. 1980, ApJ, 236, 119
Eckart, A., Downes, D., Genzel, R., Harris, A. I., Jaffe, D. T., & Wild, W. 1990, ApJ, 348, 434
Falgarone, E., Phillips, T. G., & Walker, C. 1991, ApJ, 378, 186
Flower, D. R., & Launay, J. M. 1985, MNRAS, 214, 271
Genzel, R., & Stutzki, J. 1989, ARA&A, 27, 41
Goldreich, P., & Kwan, P. 1974, ApJ, 189, 441
Güsten, R. 1989, IAU Symp. 136, The Center of the Galaxy, ed. M. Morris (Dordrecht: Kluwer), 89
Güsten, R., Serabyn, E., Kasemann, C., Schinckel, A., Schneider, G., Schulz, A., & Young, K. 1993, ApJ, 402, 537
Handa, T., Nakai, N., Sofue, Y., Hayashi, M., & Fujimoto, M. 1990, PASJ, 42, 1
Harris, A. I., Hills, R. E., Stutzki, J., Graf, U. U., Russell, A. P. G., & Genzel, R. 1991, ApJ, 382, L75
Heckathorn, H. M. 1972, ApJ, 173, 501
Hildebrand, R. H., Loewenstein, R. F., Harper, D. A., Orton, G. S., Keene, J., & Whitcomb, S. E. 1985, ApJ, 64, 64
IRAS Point Source Catalog. 1985, Joint *IRAS* Science Working Group (Washington, DC: US GPO)
Ishizuki, S., Kawabe, R., Ishiguro, M., Okumura, S. N., Morita, K.-I., Chihada, Y., & Kasugo, T. 1990, Nature, 344, 224
Israel, F. P. 1992, Leiden preprint, STW 199-92
Keel, W. C. 1984, ApJ, 282, 75
Kennicutt, R. C. 1989, ApJ, 344, 685
Knapp, G. R., Phillips, T. G., Huggins, P. J., Leighton, R. B., & Wannier, P. G. 1980, ApJ, 240, 60
Krügel, E., Chini, R., Kreysa, E., & Sherwood, W. A. 1988, A&A, 190, 47
Lada, E. A. 1992, ApJ, 339, L25
Langer, W. D., & Penzias, A. A. 1990, ApJ, 357, 477
Lebofsky, M. J., & Rieke, G. H. 1979, ApJ, 229, 111
Lester, D. F., Carr, J. S., Joy, M., & Gaffney, N. 1990, ApJ, 352, 544
Lis, D. C., & Goldsmith, P. F. 1989, ApJ, 337, 704
Loiseau, N., Nakai, N., Sofue, Y., Wielebinski, R., Reuter, H.-P., & Klein, U. 1990, A&A, 228, 331
Maddalena, R. J., Morris, M., Moscowitz, J., & Thaddeus, P. 1986, ApJ, 303, 375
Maloney, P. R., & Black, J. H. 1988, ApJ, 325, 389
Martin, R. N., & Ho, P. T. P. 1986, ApJ, 308, L7
Mauersberger, R., & Henkel, C. 1990, A&A, 236, 63
Mauersberger, R., Henkel, C., Wilson, T. L., & Harju, J. 1989, A&A, 226, L5
McCall, M. L. 1989, AJ, 97, 1341
McCarthy, P. J., Heckman, T., & van Breugel, W. 1987, AJ, 92, 264
Newton, K. 1980, MNRAS, 191, 169
Nguyen-Q-Rieu, Jackson, J. M., Henkel, C., Truong-Bach, & Mauersberger, R. 1992, ApJ, in press
Nguyen-Q-Rieu, Nakai, N., & Jackson, J. M. 1989, A&A, 220, 57
Olofsson, H., & Rydbeck, G. 1984, A&A, 136, 17
Oort, J. H. 1977, ARA&A, 15, 295
Planesas, P., Gómez-González, J., & Martín-Pintado, J. 1989, A&A, 216, 1
Rickard, L. J, Palmer, P., Morris, M., Turner, B. E., & Zuckerman, B. 1977a, ApJ, 213, 673
Rickard, L. J, Turner, B. E., & Palmer, P. 1977b, ApJ, 218, L51
Rieke, G. H., Lebofsky, M. J., Thompson, R. I., Low, F. J., & Tokunaga, A. T. 1980, ApJ, 238, 24
Rogstad, D. H., Lockhart, I. A., & Wright, M. C. H. 1974, ApJ, 193, 309
Rosenthal, E., Eales, S., Stephens, S., & Lo, K.-Y. 1990, in Internat. Symp. on Submillimeter and Millimeter Wave Astronomy, ed. G. D. Watt & A. Webster (Boston: Kluwer), 241
Sage, L. J., Mauersberger, R., & Henkel, C. 1991, A&A, 249, 31
Sanders, D. B., Scoville, N. Z., & Solomon, P. M. 1985, ApJ, 289, 373
Schinke, R., Engel, V., Buck, U., Meyer, H., & Diercksen, G. H. F. 1985, ApJ, 299, 939
Scoville, N. Z., Soifer, B. T., Neugebauer, G., Young, J. S., Matthews, K., & Yerka, J. 1985, ApJ, 289, 129
Sofue, Y., Doi, M., Ishizuki, S., Nakai, N., & Handa, T. 1988, PASJ, 40, 511
Solomon, P. M., Downes, D., & Radford, S. J. E. 1992, ApJ, 387, L55
Stacey, G. J., Geis, N., Genzel, R., Lugten, J. B., Poglitsch, A., Sternberg, A., & Townes, C. H. 1991, ApJ, 373, 423
Stark, A. A., Bally, J., Wilson, R. W., & Pound, M. W. 1989, IAU Symp. 136, The Center of the Galaxy, ed. M. Morris (Dordrecht: Kluwer), 129
Sutton, E. C., Masson, C. R., & Phillips, T. G. 1983, ApJ, 275, L49
Stutzki, J., & Güsten, R. 1990, ApJ, 356, 513
Talbot, R. J., Jensen, E. B., & Dufour, R. J. 1979, ApJ, 229, 91
Telesco, C. M., & Harper, D. A. 1980, ApJ, 235, 392
Thronson, H. A., Majewski, S., Descartes, L., & Hereld, M. 1990, ApJ, 364, 456
Tilanus, R. P. J., Tacconi, L. J., Zhou, S., Sanders, D. B., Sutton, E. C., Lo, K.-Y., Stephens, S. A., & Wynn-Williams, C. G. 1991, ApJ, 376, 500
Tully, R. B. 1988, Nearby Galaxies Catalog (Cambridge Univ. Press)
Turner, J. L., Ho, P. T. P., & Beck, S. C. 1987a, ApJ, 313, 644
Turner, J. L., Ho, P. T. P., & Martin, R. N. 1987b, in Star Formation in Galaxies, ed. C. J. L. Persson (Washington, DC: NASA CP 2466), 383
van Dishoeck, E. F., & Black, J. H. 1988, ApJ, 334, 771
van Dishoeck, E. F., Black, J. H., Phillips, T. G., & Gredel, R. 1991, ApJ, 366, 141
Wall, W. F. 1991, Ph.D. thesis, University of Texas at Austin
Wall, W. F., & Jaffe, D. T. 1990, ApJ, 361, L45
Wall, W. F., Jaffe, D. T., Israel, F. P., & Bash, F. N. 1991, ApJ, 380, 384
Wannier, P. G. 1989, in IAU Symp. 136, The Center of the Galaxy, ed. M. Morris (Dordrecht: Kluwer), 107
Weliachew, L., Casoli, F., & Combes, F. 1988, A&A, 199, 29
Wiklind, T., Rydbeck, G., Hjalmarson, Å., & Bergman, P. 1990, A&A, 232, L11
Wolfire, M. G., Hollenbach, D., & Tielens, A. G. G. M. 1989, ApJ, 344, 770
Wright, E. L. 1976, ApJ, 210, 250
Wright, E. L., et al. 1991, ApJ, 381, 200
Wright, M. C. H., & Seielstad, G. A. 1973, Astrophys. Lett., 13, 1
Young, J. S. 1987, in IAU Symp. 115, Star-forming Regions, ed. M. Peimbert & J. Jugaku (Boston: Reidel), 577
Young, J. S., & Scoville, N. Z. 1982a, ApJ, 258, 467
———. 1982b, ApJ, 260, L11
———. 1984, ApJ, 287, 153